NACA RM L50F16

NACA

RESEARCH MEMORANDUM

LOW-SPEED AERODYNAMIC CHARACTERISTICS OF A SERIES OF SWEPT WINGS HAVING NACA 65A006 AIRFOIL SECTIONS

(Revised)

By Jones F. Cahill and Stanley M. Gottlieb

Langley Aeronautical Laboratory
Langley Air Force Base, Va.

NATIONAL ADVISORY COMMITTEE
FOR AERONAUTICS

WASHINGTON

October 17, 1950

NATIONAL ADVISORY COMMITTEE FOR AERONAUTICS

RESEARCH MEMORANDUM

LOW-SPEED AERODYNAMIC CHARACTERISTICS OF A SERIES OF SWEPT WINGS HAVING NACA 65A006 AIRFOIL SECTIONS*

(Revised)

By Jones F. Cahill and Stanley M. Gottlieb

SUMMARY

An investigation was made to determine the effect of sweep, taper ratio, and aspect ratio on the aerodynamic characteristics of nine semispan wings of NACA 65A006 airfoil section with and without split flaps. Lift, drag, pitching-moment, and wing-root bending-moment characteristics were measured through a range of Reynolds numbers from 1.5×10^6 to 12.0×10^6. One of these wings was tested with a hinged leading-edge flap of various spans and deflections to determine the effect of this type of flap on longitudinal stability near maximum lift.

For wings of aspect ratio 4, increases in sweep angle increased the maximum lift coefficient of the plain wings but decreased the maximum lift coefficient of the wings with half-span split flaps. Rather abrupt unstable changes in pitching moment occurred at lift coefficients well below maximum for nearly all of the swept wings tested. Increases in sweep angle or aspect ratio reduced the lift coefficient at which these unstable changes occurred. Increases in lift-curve slope and stable changes in pitching moment occurring at low to moderate lift coefficients for the sweptback wings were increased in magnitude by increase in taper ratio and decrease in aspect ratio. Reynolds number effects were confined to the more highly sweptback wings at low to moderate lift coefficients.

INTRODUCTION

The use of sweep to delay the effects of compressibility on the aerodynamic characteristics of airplane wings has given rise to a need for data on swept wings at both low and high speeds to aid designers in

* Originally issued March 24, 1950 as NACA RM L9J20.

their evaluation of wing characteristics. Previous investigations, references 1 and 2, for instance, have indicated pronounced scale effects on the characteristics of swept wings with other than sharp leading edges. It is desirable, therefore, that data for these wings should be obtained at Reynolds numbers as near as possible to those at which the wings are expected to be used. A number of investigations of the characteristics of swept wings at high Reynolds numbers have been made, but as yet there does not exist any related data from which the individual effects of the plan-form variables can be evaluated.

An investigation has been started in the Langley two-dimensional low-turbulence pressure tunnel to study, at relatively high Reynolds numbers, the effects of systematic variations in wing geometry on the low-speed aerodynamic characteristics of wings for high-speed airplanes. The present paper presents the results of tests of a series of nine wings having NACA 65A006 sections, covering a range of sweep angles from -45° to 60°, aspect ratios from 2 to 6, and taper ratios from 0.3 to 1.0. Tests were made of the wings alone and with half-span split flaps at Reynolds numbers from 1.5×10^6 to 12×10^6.

One of these wings, of aspect ratio 4 and with 45° sweepback of the quarter-chord line, was tested with a hinged leading-edge flap of various spans to determine the effect of this type of flap on longitudinal stability at the stall.

SYMBOLS

C_L lift coefficient $\left(\frac{\text{Twice model lift}}{qS}\right)$

$C_{L_{max}}$ maximum lift coefficient

C_{L_s} highest lift coefficient reached before unstable pitching-moment break

C_D drag coefficient $\left(\frac{\text{Twice model drag}}{qS}\right)$

C_M pitching-moment coefficient $\left(\frac{\text{Twice model pitching moment}}{qS\bar{c}}\right)$

C_B wing-root bending-moment coefficient $\left(\frac{B}{q\frac{S}{2}\frac{b}{2}}\right)$

B bending moment at wing root, foot-pounds

q free-stream dynamic pressure $\left(\frac{1}{2}\rho V_o^2\right)$

ρ free-stream mass density, slugs per cubic foot

V_o free-stream velocity, feet per second

S twice model area, square feet

b twice model span, feet

A aspect ratio of complete wing $\left(\frac{b^2}{S}\right)$

$\bar{c}$ mean aerodynamic chord, feet $\left(\frac{2}{S}\int_0^{b/2} c^2 dy\right)$

c wing chord at any spanwise station, feet

Λ sweep of wing quarter-chord line

λ wing taper ratio $\left(\frac{C_T}{C_R}\right)$

α angle of attack of wing chord line, degrees

R Reynolds number $\left(\frac{\rho V \bar{c}}{\mu}\right)$

C_{L_α} rate of change of lift coefficient with angle of attack, degrees

C_T chord of tip parallel to plane of symmetry, feet

C_R chord of root parallel to plane of symmetry, feet

$\bar{y}$ spanwise distance from plane of symmetry to $\bar{c}/4$

$\bar{x}$ distance along root chord from leading edge to $\bar{c}/4$ parallel to plane of symmetry

$(x/\bar{c})_{cp}$ nondimensional location of chordwise center of pressure, referred to $\bar{c}/4$

y distance along semispan

δ flap deflection (in plane of symmetry), degrees

η nondimensional spanwise location $\left(\frac{y}{b/2}\right)$

η_{cp} nondimensional location of spanwise center of pressure

MODELS

The semispan models tested all had NACA 65A006 airfoil sections parallel to the plane of symmetry and no twist or dihedral. The plan-form characteristics of the nine wings tested and some of the principal dimensions are shown in figure 1. The wing tips were rounded off both in plan form and cross section beginning at $0.975\frac{b}{2}$.

For the sake of brevity, a system of designating these wings similar to that suggested in reference 3 has been adopted which includes the sweep angle, aspect ratio, and taper ratio. The designation 45–4–0.6, for instance, designates a wing whose quarter-chord line is swept back 45°, with an aspect ratio of 4 and a taper ratio of 0.6.

The following is a list of the wings tested:

–45–4–0.6	45–2–0.6	45–4–0.3
0–4–0.6	(45–4–0.6)	(45–4–0.6)
30–4–0.6	45–6–0.6	45–4–1.0
45–4–0.6		
60–4–0.6		

The central configuration (45–4–0.6) has been placed in parentheses in the last two columns, since the designation is merely repeated to show the complete series of variables.

The models were constructed of aluminum alloy and were polished to a smooth finish. Each of the models could be fitted with a 0.20c half-span inboard trailing-edge split flap deflected 60° in the plane of symmetry. The flaps were made of bent sheet metal approximately 1/16 inch thick.

One of the models (the 45-4-0.6) was equipped with a hinged leading-edge flap as shown in figure 2. The chord of the flap was 0.15c and could be deflected to various angles in sections along the span. The deflections, which were measured perpendicular to the hinge line, were set with plates, screwed to the upper surface of the wing and flap, having a radius equal to the distance from the hinge line to the wing upper surface and faired into both the wing and the flap contours. With the leading-edge flap deflected, tests were also made with fences on the upper surface of the wing. The fences were made of sheet metal approximately 1/32 inch thick and 1/2 inch high. The shape and locations of the fences are also shown in figure 2. Photographs of the 45-4-0.6 wing with and without leading-edge flaps and fences are shown in figure 3.

For model configurations with leading-edge roughness, 0.004-inch-diameter carborundum particles were imbedded in a thin coat of shellac over a length of 0.08c from the leading edge on both surfaces.

TESTS

The tests of the semispan models were made in the Langley two-dimensional low-turbulence pressure tunnel with a four-component electrical resistance-type strain-gage balance. The validity of data obtained in this semispan arrangement has been established by means of tests of a model of a wing which had previously been tested in a full-span arrangement in the Langley 19-foot pressure tunnel (reference 4).

Each of the models was tested with and without half-span split trailing-edge flaps both in the smooth condition and with leading-edge roughness. Lift, drag, pitching-moment, and wing-root bending-moment data were measured from below zero lift to above the stall for most of the wings in the smooth condition through a range of Reynolds numbers varying from 3.0×10^6 to 12.0×10^6. Tests of the 45-4-0.6, 60-4-0.6, 45-4-1.0, and 45-6-0.6 wings were limited to lower Reynolds numbers because of strength limitations of the models. The effects of leading-edge roughness on the aerodynamic characteristics of the wings were determined at one Reynolds number for each model. Tests were made of the 45-4-0.6 wing equipped with a hinged leading-edge flap of various spans and deflections at a Reynolds number of 4.5×10^6 to determine the effect of the flap deflection and span on longitudinal stability at the

stall. Fences were tested on the wing with one leading-edge-flap configuration in an attempt to delay spanwise flows.

Drag coefficients and angles of attack were corrected for jet-boundary effects by means of boundary-induced upwash corrections calculated by the method of reference 5.

The highest Mach number attained during these tests was approximately 0.20.

PRESENTATION OF DATA

The aerodynamic characteristics of the wings tested with and without split flap and roughness are presented in figures 4 to 12. Figures 13 to 17 present data showing the effect of leading-edge-flap deflection and span on the aerodynamic characteristics of the 45-4-0.6 wing with and without split flaps and fences. These data are presented as plots of angle of attack, root bending-moment coefficient, pitching-moment coefficient, and drag coefficient against lift coefficient.

The figures in which the data for the various wings are presented are listed in the following table:

-45-4-0.6	figure 4	45-4-0.3	figure 9
0-4-0.6	figure 5	45-4-1.0	figure 10
30-4-0.6	figure 6	45-2-0.6	figure 11
45-4-0.6	figure 7	45-6-0.6	figure 12
60-4-0.6	figure 8		

Summary plots of the effect of sweep angle, aspect ratio, and taper ratio on certain aerodynamic characteristics of the wings tested are presented in figures 18 to 22. The theoretical values of lift-curve slope, aerodynamic center, and spanwise center of pressure of the additional load, obtained from reference 6, are presented in figures 18, 21, and 22, respectively.

RESULTS AND DISCUSSION

Characteristics of Wings Alone and with Half-Span Split Flaps

General description of vortex-flow phenomena over sweptback wings with small leading-edge radii.- Several investigations have been made into the nature of the air flow about swept wings having small leading-edge radii (references 2, 7, and 8). It is believed that a brief review of some of the more important results of these studies will aid in the interpretation of the results obtained on the wings of the present investigation. These investigations have shown that leading-edge separation occurs at relatively low angles of attack and spreads rapidly along the span as the angle of attack is increased. Generally the flow closes in again behind the initial separation and forms a "bubble" of separated flow.

The pressure-distribution data in reference 7 show no apparent separation at the wing root but a region of separated flow at other spanwise stations which increases in chordwise extent toward the wing tip. As the angle of attack is increased, the portion of the chord covered by the separated region increases until, at some angle of attack, the sections near the tip are completely separated. Further increases in angle of attack cause increases in the extent of the completely separated portion of the span.

Reference 8 shows that a strong vortex is formed within this bubble and that, at low angles of attack, the core of the vortex lies along a line passing through the leading edge of the root chord and swept back slightly more than the wing leading edge. As the angle of attack is increased, the sweep angle of the vortex core increases and the portion of the vortex core near the wing tip curves back in the stream direction. Comparisons between the pressure distributions for a wing with a sharp leading edge and a wing with NACA 65-006.5 airfoil sections show that the strength of the vortex is greater for the wing with the sharp leading edge. An investigation of the flow about a wing of approximately triangular plan form (reference 2) showed that the vortex flow was evident on a wing with 15-percent-thick airfoil sections with rounded leading edges at low Reynolds numbers but not at high Reynolds numbers. These data also show that the vortex flow existed at both Reynolds numbers when the wing had sharp leading edges.

In a number of instances, the formation of this separation-vortex-flow pattern is accompanied by an increase in lift-curve slope. It may be assumed that this increase in lift is caused by the fact that the stream must flow effectively about a thick, highly cambered airfoil. These increases in lift could be expected to exist until the angle of attack had been increased to the point where complete separation exists over the tip sections. The loss in lift associated with the complete

separation should then cause the lift-curve slope to decrease. The results presented in reference 2 show rather strikingly the fact that the maximum lift coefficient as well as the lift-curve slope may be increased appreciably by the presence of the separation-vortex-flow pattern.

No visual observations were made of the flow characteristics for the wings of the present investigation. In view of the relatively small thickness ratio and leading-edge radius of these wings, however, it is believed that a similar separation-vortex-flow pattern exists for the more highly swept wings tested. No conclusive evidence of this type of flow is apparent in the case of the wings with sweep angles less than 45°. The data for the sweptforward wing show effects similar to those caused by the vortex on the sweptback wings although it would seem that the flow phenomena would be different in some respects from that observed on sweptback wings.

Lift-curve slopes.- An examination of the data for the various wings shows that at low Reynolds numbers large increases in lift-curve slopes of the swept wings occurred at moderate angles of attack. (See, for example, figs. 7(a) and 8(a).) The magnitude of these changes in lift-curve slopes increased as sweep angle or taper ratio were increased and as aspect ratio was decreased. No change was noted for the wing of zero sweep. As the Reynolds number was increased, the magnitude of these changes in lift-curve slope generally decreased, or at least the change in slope was delayed to higher angles of attack. It would seem that this delay in the change in lift-curve slope indicates a delay in the formation of the separation "bubble" as the Reynolds number was increased. This agrees, at least qualitatively, with the scale effect previously noted for the wings of triangular plan form and round leading edges (reference 2).

Although the lift-curve slopes at moderate angles of attack showed rather large variations with changes in Reynolds number, the variation of Reynolds number had very little effect on the lift-curve slope near zero angle of attack. Lift-curve slopes (near zero angle of attack) are shown plotted against sweep angle, aspect ratio, and taper ratio in figure 18. The general trends of the variations with changes in the plan-form parameters are shown to agree with those shown by the theoretical values taken from reference 6, although for moderate sweep angles the absolute values are not always in good agreement. The data with leading-edge roughness show that generally the effect of roughness on lift-curve slope is small and the shape of the lift curves obtained with leading-edge roughness agrees fairly closely with that obtained for the smooth wing at the same Reynolds number.

Maximum lift.- Maximum lift coefficients of the wings tested at a Reynolds number of 3.0×10^6 with and without half-span split flaps are shown in figure 19(a). These data show large increases in maximum lift

coefficient of the plain wings as the sweep is increased either positively or negatively. The flap effectiveness decreases, however, as the sweep is increased and the resulting maximum lift coefficients with split flaps decrease with increase in positive sweep angle. In fact, for the 60° sweptback wing the addition of split flaps actually decreased the maximum lift coefficient. With a sweepback angle of 45° and taper ratio of 0.6 the maximum lift coefficient decreased slightly with increasing aspect ratio from 2 to 6, but with 45° of sweepback and an aspect ratio of 4 the change in maximum lift coefficients with a change in taper ratio from 0.3 to 1.0 was negligible. The flap effectiveness on the maximum lift coefficient was negligible for a sweepback angle of 45° regardless of aspect ratio or taper ratio.

In many cases, however, the pitching-moment curves break in an unstable direction at lift coefficients well below the maximum. The highest lift coefficient reached before these unstable changes in pitching moments take place (C_{L_s}) are shown plotted against sweep angle, aspect ratio, and taper ratio in figure 19(b). No unstable change in pitching-moment slope occurred for the wings of 0° and 30° of sweep or for the 45° sweptback wing of aspect ratio 2 so the actual maximum lift coefficients are plotted for these wings. For sweep angles greater than 30°, increases in sweep angle or in aspect ratio decrease the lift coefficient at which the unstable break takes place; whereas changes in taper ratio have little effect. The addition of the half-span split flap increases the lift coefficient at which the pitching moments break unstable for all of the wings except the 45° sweptforward.

The effects of variation in Reynolds number on either maximum lift coefficient or on the lift coefficient for the unstable pitching-moment break were small in all cases except for the 30° sweptback wing (fig. 6) which showed a higher maximum lift coefficient at a Reynolds number of 6×10^6 than for Reynolds numbers either above or below this value. This phenomena must be associated with some peculiar scale effect on the laminar flow around the leading edge since the addition of leading-edge roughness decreased the maximum lift to approximately the value obtained at other Reynolds numbers. Aside from this isolated instance, leading-edge roughness has very little effect on the lift characteristics of any of the wings tested.

The effects of changes in airfoil section on the lift coefficient at which the unstable pitching-moment break occurs may be deduced from a comparison of these data with other previously published data. Data for a wing having plan-form parameters (40-4-0.625) roughly similar to the 45-4-0.6 wing tested in this investigation but with circular-arc sections are presented in reference 9. These data show that the lift coefficient at which the unstable pitching-moment break occurs is approximately the same for the circular-arc wing as for the

6-percent-thick low-drag wing. Data in references 10 and 11 for two wings (40-4-0.625 and 50-2.9-0.625) having airfoil sections 9.6 and 7.8 percent thick, respectively, (and, therefore, larger leading-edge radii than the 6-percent-thick wings) show that the pitching-moment break occurs at appreciably higher lift coefficients than would be indicated by the data of the present investigation for wings of roughly similar plan form and 6-percent-thick sections. It seems likely therefore that, for wings swept back approximately 45°, the changes in leading-edge radius corresponding to decreases in thickness ratio below 6 percent will have little effect on the lift coefficient at which the pitching moments break unstable but that this lift coefficient may be raised substantially by relatively small increases in thickness.

Pitching moments.- An examination of the pitching-moment data in figures 4 to 12 shows that abrupt variations in the slope of the pitching-moment curve occur at lift coefficients well below maximum lift for nearly all of the wings tested. In all cases except the 0-4-0.6, the 30-4-0.6, and the 45-2-0.6 wings, unstable variations occurred. These changes in pitching-moment characteristics are in agreement with the boundary curve for stability at high lift coefficients presented in reference 12. The unstable changes in the pitching-moment curves occur at the same lift coefficient as the shifts in the spanwise center of pressure (fig. 20), which would indicate that this instability can be attributed to complete separation over the tip sections of the swept-back wings. The inboard movements of spanwise center of pressure shown in figure 20 indicate appreciable tip stalling even for those sweptback wings for which there are no unstable variations in the pitching moment.

At lift coefficients below those at which the unstable pitching-moment changes occur, smaller changes in pitching moment which are generally in a stable direction can be noticed in the data for the sweptback wings. These stable changes begin at approximately the same lift coefficient as the increases in lift-curve slope and are apparently a result of the separation-vortex-flow pattern. The previously noted stable breaks in pitching moment at maximum lift for the 0-4-0.6, 30-4-0.6, and 45-2-0.6 wings seem to be caused by the final complete stall but, for the 45° sweptback wing of aspect ratio 2 at least, the gradual change in the stable direction at lower lift coefficients should be attributed to the action of the vortex. Decreases in aspect ratio and increases in taper ratio cause increases in the magnitude of the stable change. These effects of change in plan form are identical to the previously noted effects of changes in plan form on the lift-curve slope increase. The center-of-pressure data presented in figure 20 show that the stable changes in pitching moment can be attributed to rearward shifts in the chordwise centers of pressure which are accompanied by relatively small or erratic shifts in spanwise center of pressure. These rearward shifts in center of pressure are probably caused by the

fact that the leading-edge separation decreases the magnitude of the leading-edge pressure peaks while the chordwise extent of the decreased pressure increases (reference 7).

In general, the observations made above for the unflapped wing apply to the data for the wings with half-span split flaps also. In the range of lift coefficients where the stable changes in pitching moments occur, the changes in pitching-moment characteristics which occur as a result of the addition of leading-edge roughness are small. The slopes of the pitching-moment curves seem to show fair agreement with aerodynamic-center positions given in reference 6 (see fig. 21) except for the 60° wing which shows a more forward aerodynamic-center position than the 45° wing, whereas the theory would indicate a rearward shift.

A consideration of the loading added by deflection of the half-span split flaps on the various wings indicates that increasing angle of sweepback, aspect ratio, or taper ratio will cause the centroid of the added load to move forward with respect to the quarter-chord point of the mean aerodynamic chord. The data show that increasing any of the three plan-form parameters does cause a decrease in the negative pitching-moment increment caused by flap deflection and that positive increments in pitching moments at zero lift actually result from deflecting the flaps on the 60° sweptback wing and the 45° sweptback wing of aspect ratio 6.

Drag characteristics.- The induced drag polar has been plotted on figure 10(a) to show a typical variation in the magnitude of the profile drag coefficients. The lift coefficient at which appreciable divergence between the induced drag polar and experimental values of drag coefficient begins agrees quite closely with the lift coefficient at which the lift-curve slope begins to increase. The increase in drag at this point could be expected because of the large decrease in the value of the peak negative pressure accompanying leading-edge separation.

Wing-root bending moments.- The data for these wings show that the wing-root bending moments are roughly linear up to about the lift coefficient at which the pitching-moment break occurs. The spanwise centers of pressure shown in figure 20 help to show the changes which take place in the loading on the wings. The spanwise centers of pressure are generally constant at moderate lift coefficients and move rather rapidly inboard for the sweptback wings and outboard for the sweptforward wing at high lift coefficients.

Values of the spanwise center of the additional load distribution, indicated by the slope of the bending-moment curve through zero lift, are shown plotted against the various plan-form parameters in figure 22.

These data show good agreement with calculated values except for the wing with aspect ratio 6 and the wing with taper ratio 0.3. In both of these cases, the spanwise center of pressure is farther inboard than indicated by the computations.

Characteristics of 45–4–0.6 Wing with Hinged Leading–Edge Flap

Data are shown in figures 13 to 17 on the characteristics of the 45–4–0.6 wing equipped with a hinged leading–edge flap at a Reynolds number of 4.5×10^6 both with and without half–span split flap. Deflections of 10°, 20°, 30°, and 40° were tested for leading–edge–flap spans ranging from $0.37\frac{b}{2}$ to full span. These data show that the full–span leading–edge flap deflected 30° provided a desirable variation of pitching moments up to the highest lift coefficients of any of the combinations of leading–edge–flap span and deflection tested (about 1.1 with half–span split flap deflected). None of the configurations tested however provided stable pitching–moment variations throughout the entire range of lift coefficients. It may be noted that the half–span leading–edge flap deflected 30° provided a stable variation in pitching moments at high lift coefficients although the over–all pitching–moment variation could not be considered desirable. Use of the leading–edge flap also provided appreciable reductions in drag at high lift coefficients.

In an attempt to delay spanwise flows and, therefore, improve the pitching–moment variation at high lift coefficients, chordwise fences were installed on the wing with the $0.75\frac{b}{2}$ leading–edge flap deflected 30°. Use of the fences at the positions tested increased the maximum lift coefficient and the lift coefficient for the pitching–moment break slightly but caused no improvement in the direction of the pitching–moment break at stall.

Data for a number of sweptback wings equipped with leading–edge high–lift devices are contained in references 9 to 11 and 13 and 14. The data for a wing of aspect ratio 3.5, sweepback of 45°, and circular–arc section (reference 14) show that none of the configurations of leading–edge–flap span and deflections investigated provided completely satisfactory longitudinal stability characteristics throughout the entire lift–coefficient range. A hinged leading–edge flap covering 50 percent of the span produced stable moments at the stall for a 35° sweptback wing of aspect ratio 6 with NACA 64_1–112 airfoil section, but only when used in conjunction with a fence at 50 percent of the semispan (reference 13). Data in references 9, 10, and 13 show that extensible

leading-edge flaps, on the other hand, are capable of producing stable pitching-moment variations at the stall for wings having sweepback angles of 35° and 40° and NACA low-drag airfoil sections and for a wing having a sweepback angle of 40° and circular-arc section, whereas a 50° sweptback wing with low-drag airfoil (reference 11) requires a fence to obtain stable pitching-moment variations at stall. It seems likely therefore that a properly designed extensible leading-edge flap should provide stable pitching-moment variations for the wing tested in this investigation (45-4-0.6).

CONCLUSIONS

The results of an investigation to determine the effect of sweep, taper ratio, and aspect ratio on the aerodynamic characteristics of wings with an NACA 65A006 airfoil section led to the following conclusions:

(1) The trends of variations in lift-curve slopes, aerodynamic-center positions, and spanwise centers of pressure for low lift coefficients agree fairly well with those predicted by means of existing methods of calculation.

(2) For the wings with larger sweep angles, increases in lift-curve slopes and stable changes in pitching-moment slopes occur at moderate lift coefficients, apparently as a result of a vortex-flow pattern over the wing following leading-edge separation. These changes are increased in magnitude by increases in taper ratio or decreases in aspect ratio.

(3) Rather abrupt unstable changes in pitching moments take place at lift coefficients well below maximum for nearly all of the highly swept wings. Increases in sweep angle or aspect ratio decrease the lift coefficients at which this unstable break occurs; whereas changes in taper ratio cause relatively small changes. Deflection of a half-span split flap increases the lift coefficient for the unstable break for all of the wings tested except the 45° sweptforward wing.

(4) Increases in sweep angle cause increases in maximum lift coefficient of the unflapped wings for either positive or negative sweep. Flap effectiveness on maximum lift decreases as the sweep angle is increased and is actually negative for positive sweep angles greater than 45°. Increasing aspect ratio of a 45° sweptback wing decreases maximum lift, but changes in taper ratio have little effect.

(5) Deflection of a full-span hinged leading-edge flap 30° provides the largest increase in the lift coefficient for the unstable

pitching-moment break of any of the combinations of leading-edge-flap span and deflection tested but did not produce a stable pitching-moment variation at the stall.

(6) Scale effects on aerodynamic characteristics were confined to the more highly swept wings and consisted principally of a delay in the lift coefficient at which the increase in lift-curve slope occurs.

Langley Aeronautical Laboratory
National Advisory Committee for Aeronautics
Langley Air Force Base, Va.

REFERENCES

1. Sweberg, Harold H., and Lange, Roy H.: Summary of Available Data Relating to Reynolds Number Effects on the Maximum Lift Coefficients of Swept-Back Wings. NACA RM L6L20a, 1947.

2. Wilson, Herbert A., Jr., and Lovell, J. Calvin: Full-Scale Investigation of the Maximum Lift and Flow Characteristics of an Airplane Having Approximately Triangular Plan Form. NACA RM L6K20, 1947.

3. Schuldenfrei, Marvin, Comisarow, Paul, and Goodson, Kenneth W.: Stability and Control Characteristics of an Airplane Model Having a 45.1° Swept-Back Wing with Aspect Ratio 2.50 and Taper Ratio 0.42 and a 42.8° Swept-Back Horizontal Tail with Aspect Ratio 3.87 and Taper Ratio 0.49. NACA RM L7B25, 1947.

4. Cahill, Jones F.: Comparison of Semispan Data Obtained in the Langley Two-Dimensional Low-Turbulence Pressure Tunnel and Full-Span Data Obtained in the Langley 19-Foot Pressure Tunnel for a Wing with 40° Sweepback of the 0.27-Chord Line. NACA RM L9B25a, 1949.

5. Katzoff, S., and Hannah, Margery E.: Calculation of Tunnel-Induced Upwash Velocities for Swept and Yawed Wings. NACA TN 1748, 1948.

6. DeYoung, John: Theoretical Additional Span Loading Characteristics of Wings with Arbitrary Sweep, Aspect Ratio, and Taper Ratio. NACA TN 1491, 1947.

7. Lange, Roy H., Whittle, Edward F., Jr., and Fink, Marvin P.: Investigation at Large Scale of the Pressure Distribution and Flow Phenomena over a Wing with the Leading Edge Swept Back 47.5° Having Circular-Arc Airfoil Sections and Equipped with Drooped-Nose and Plain Flaps. NACA RM L9G15, 1949.

8. Anderson, Adrien E.: Chordwise and Spanwise Loadings Measured at Low Speed on Large Triangular Wings. NACA RM A9B17, 1949.

9. Neely, Robert H., and Koven, William: Low-Speed Characteristics in Pitch of a 42° Sweptback Wing with Aspect Ratio 3.9 and Circular-Arc Airfoil Sections. NACA RM L7E23, 1947.

10. Graham, Robert R., and Conner, D. William: Investigation of High-Lift and Stall-Control Devices on an NACA 64-Series 42° Sweptback Wing with and without Fuselage. NACA RM L7G09, 1947.

11. Foster, Gerald V., and Fitzpatrick, James E.: Longitudinal-Stability Investigation of High-Lift and Stall-Control Devices on a 52° Sweptback Wing with and without Fuselage and Horizontal Tail at a Reynolds Number of 6.8×10^6. NACA RM L8I08, 1948.

12. Shortal, Joseph A., and Maggin, Bernard: Effect of Sweepback and Aspect Ratio on Longitudinal Stability Characteristics of Wings at Low Speeds. NACA TN 1093, 1946.

13. Koven, William, and Graham, Robert R.: Wind-Tunnel Investigation of High-Lift and Stall-Control Devices on a 37° Sweptback Wing of Aspect Ratio 6 at High Reynolds Numbers. NACA RM L8D29, 1948.

14. Guryansky, Eugene R., and Lipson, Stanley: Effect of High-Lift Devices on the Longitudinal and Lateral Characteristics of a 45° Sweptback Wing with Symmetrical Circular-Arc Sections. NACA RM L8D06, 1948.

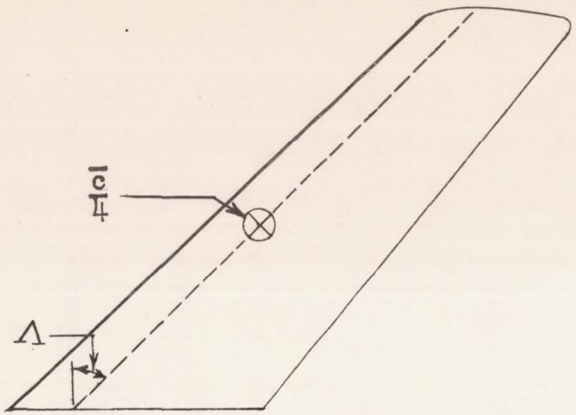

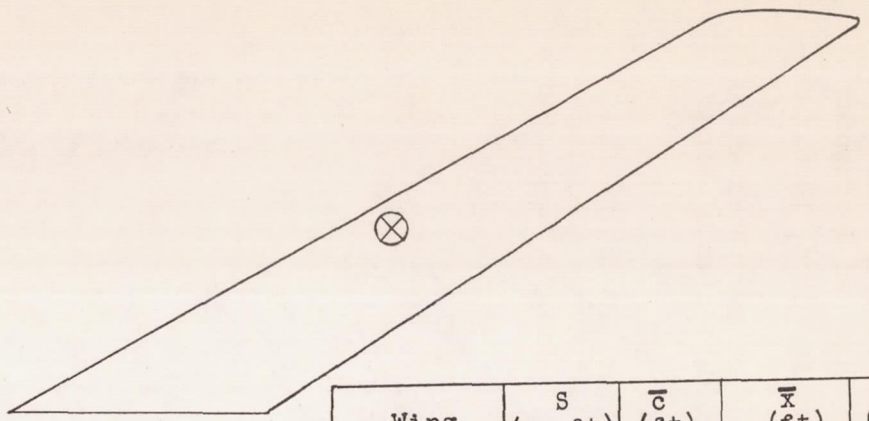

Wing	S (sq ft)	$\bar{c}$ (ft)	$\bar{x}$ (ft)	$\bar{y}$ (ft)
-45-4-0.6	1.389	.851	.503	.756
0-4-0.6	1.389	.851	-.261	.756
30-4-0.6	1.389	.851	-.702	.756
45-4-0.6	1.389	.851	-1.024	.756
60-4-0.6	1.389	.851	-1.584	.756

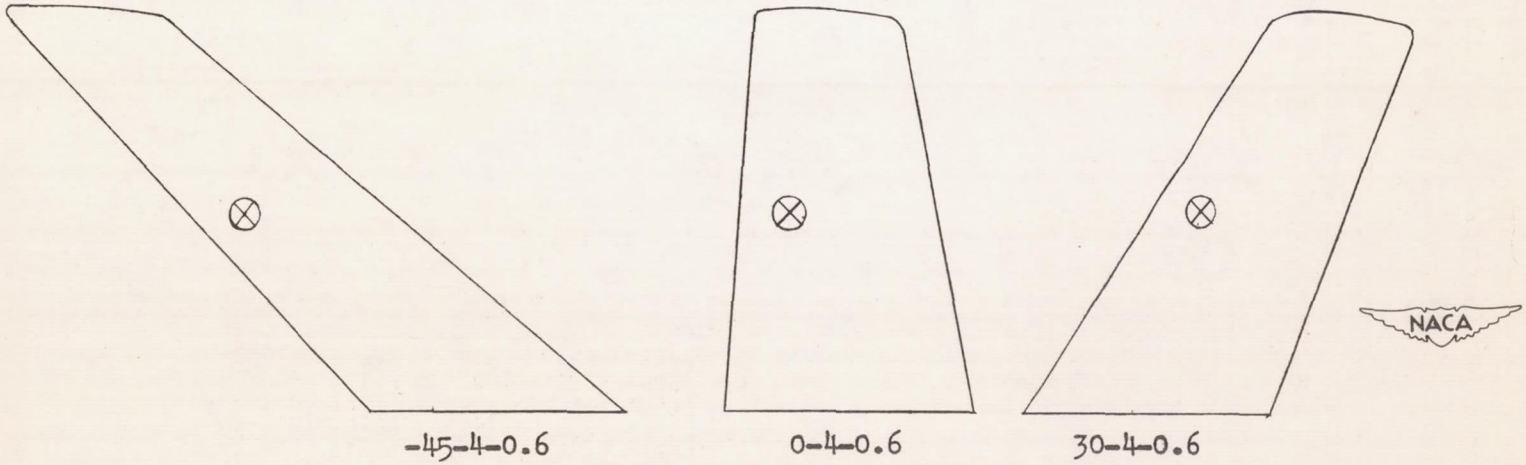

Variation in sweep angle

Figure 1.- Plan-form characteristics of wings tested.

Wing	S (sq ft)	$\bar{c}$ (ft)	$\bar{x}$ (ft)	$\bar{y}$ (ft)
45-4-0.3	1.389	.913	-1.077	.684
45-4-0.6	1.389	.851	-1.024	.756
45-4-1.0	1.389	.834	-1.045	.833
45-2-0.6	1.139	1.089	-.822	.489
45-6-0.6	1.333	.681	-1.129	.917

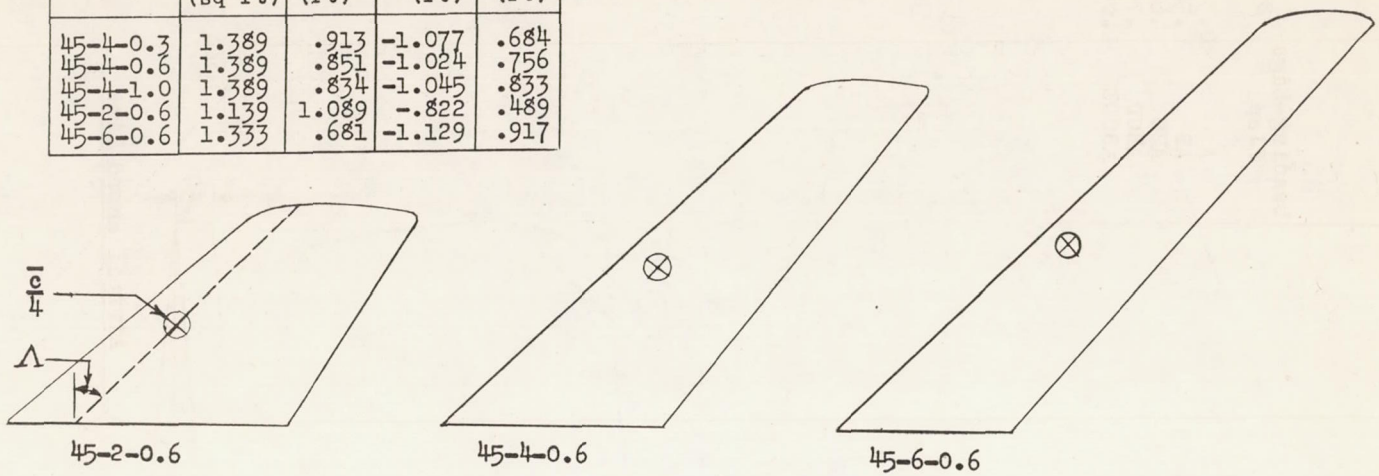

Variation in aspect ratio

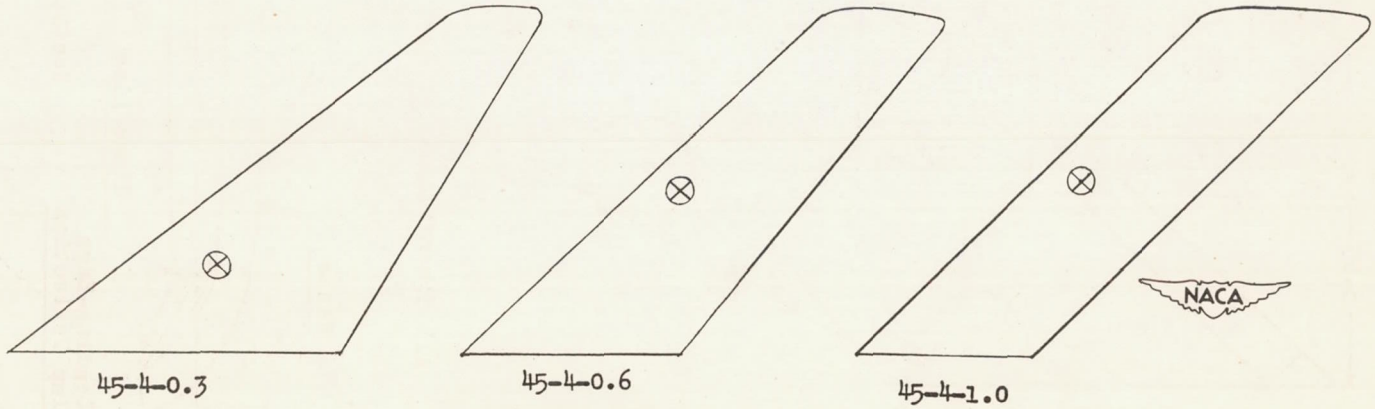

Variation in taper ratio

Figure 1.- Concluded.

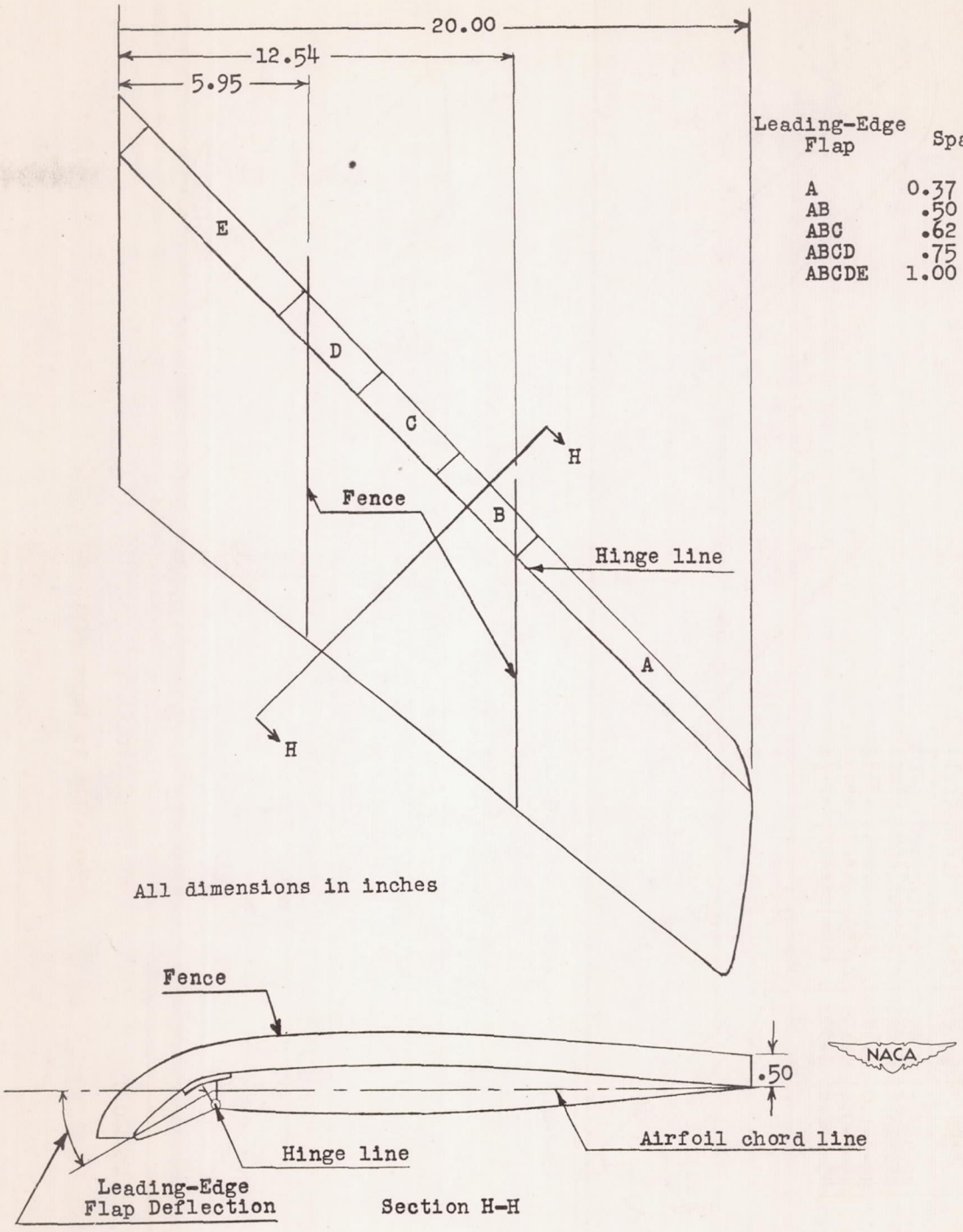

Figure 2.- Leading-edge flap and fences on 45° sweptback wing.

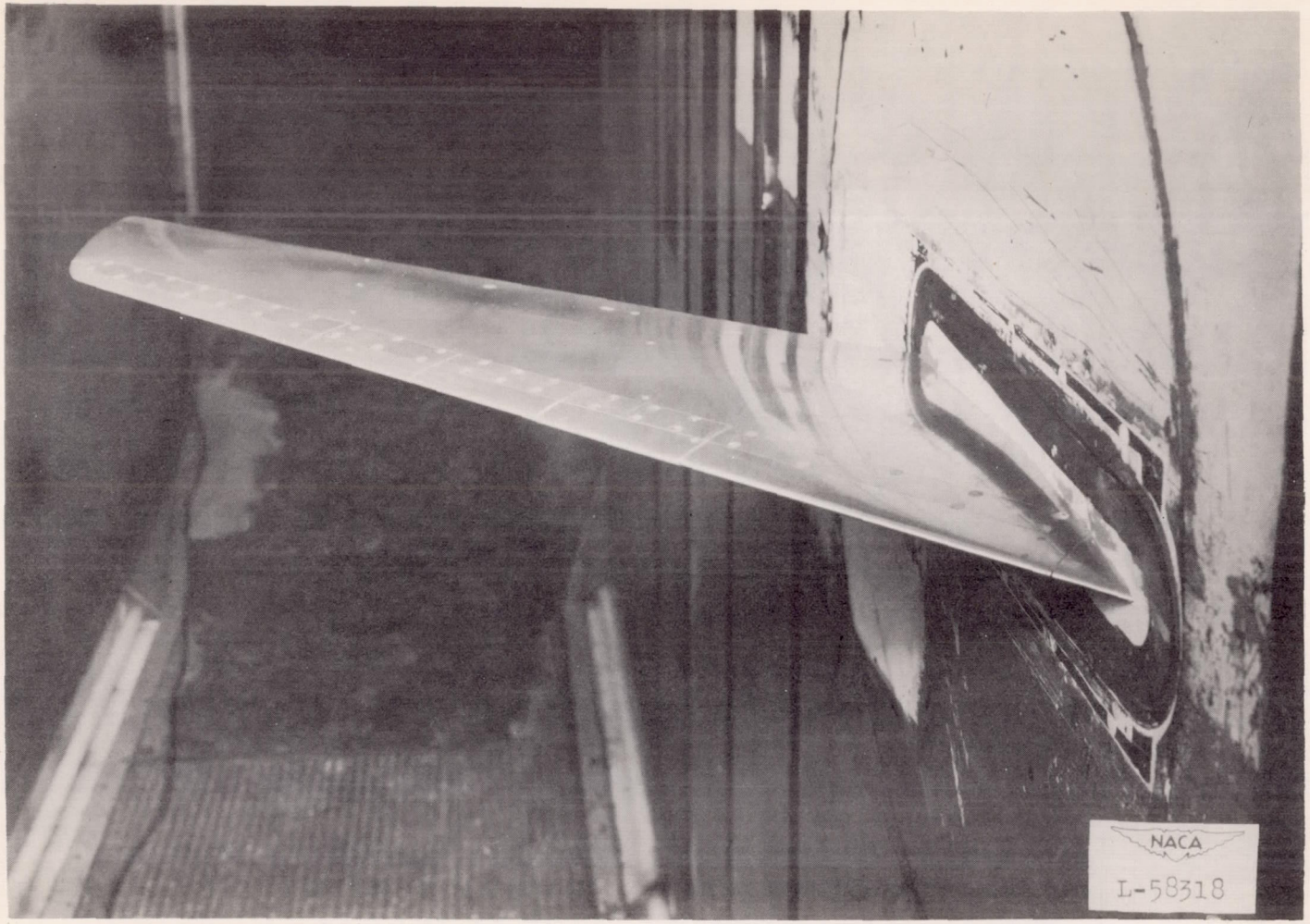

(a) Leading-edge flap retracted.

Figure 3.- The 45-4-0.6 wing model installed in Langley two-dimensional low-turbulence pressure tunnel.

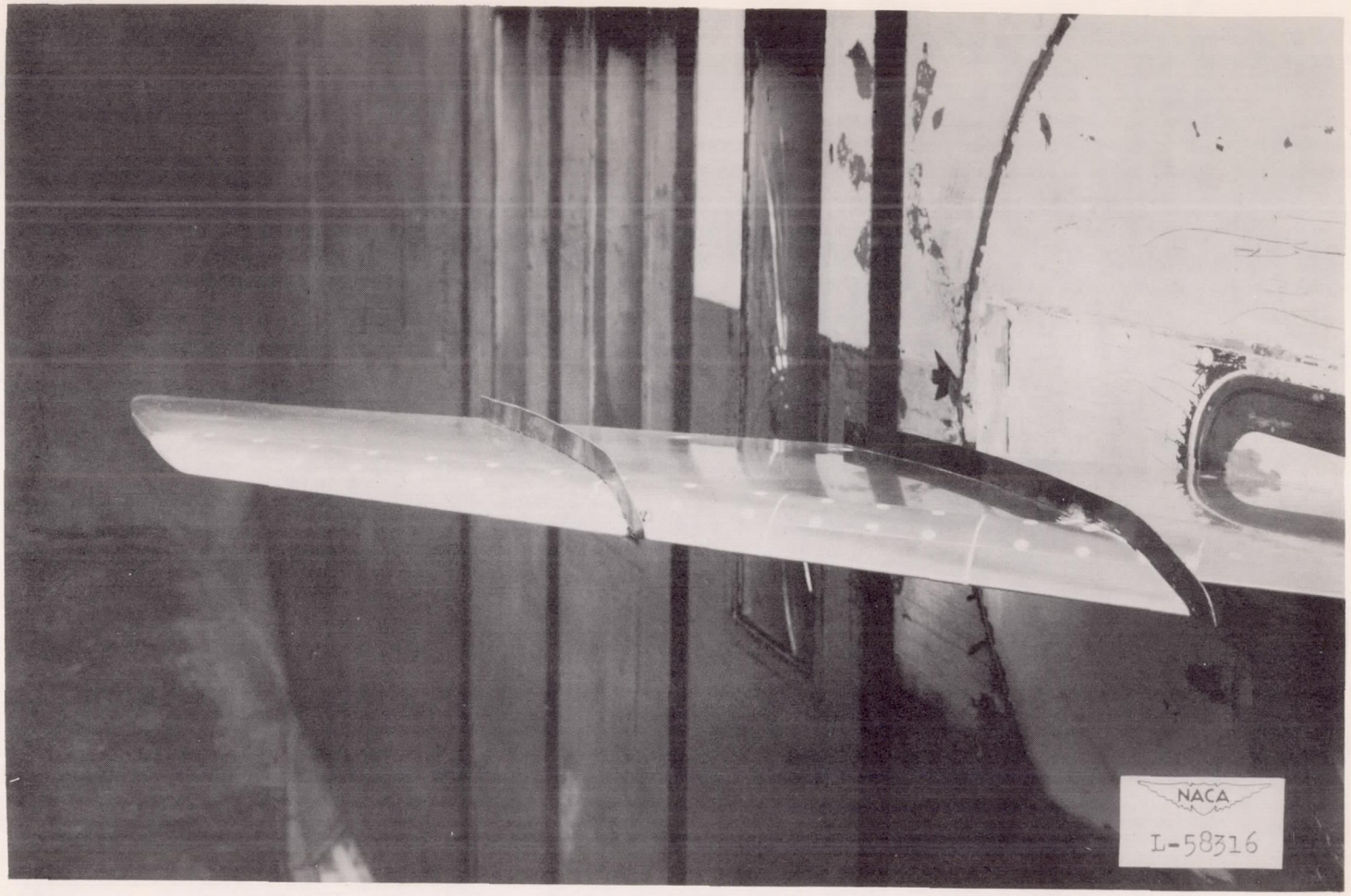

(b) Wing with $0.75\frac{b}{2}$ leading-edge flap deflected 30° and with fences.

Figure 3.- Concluded.

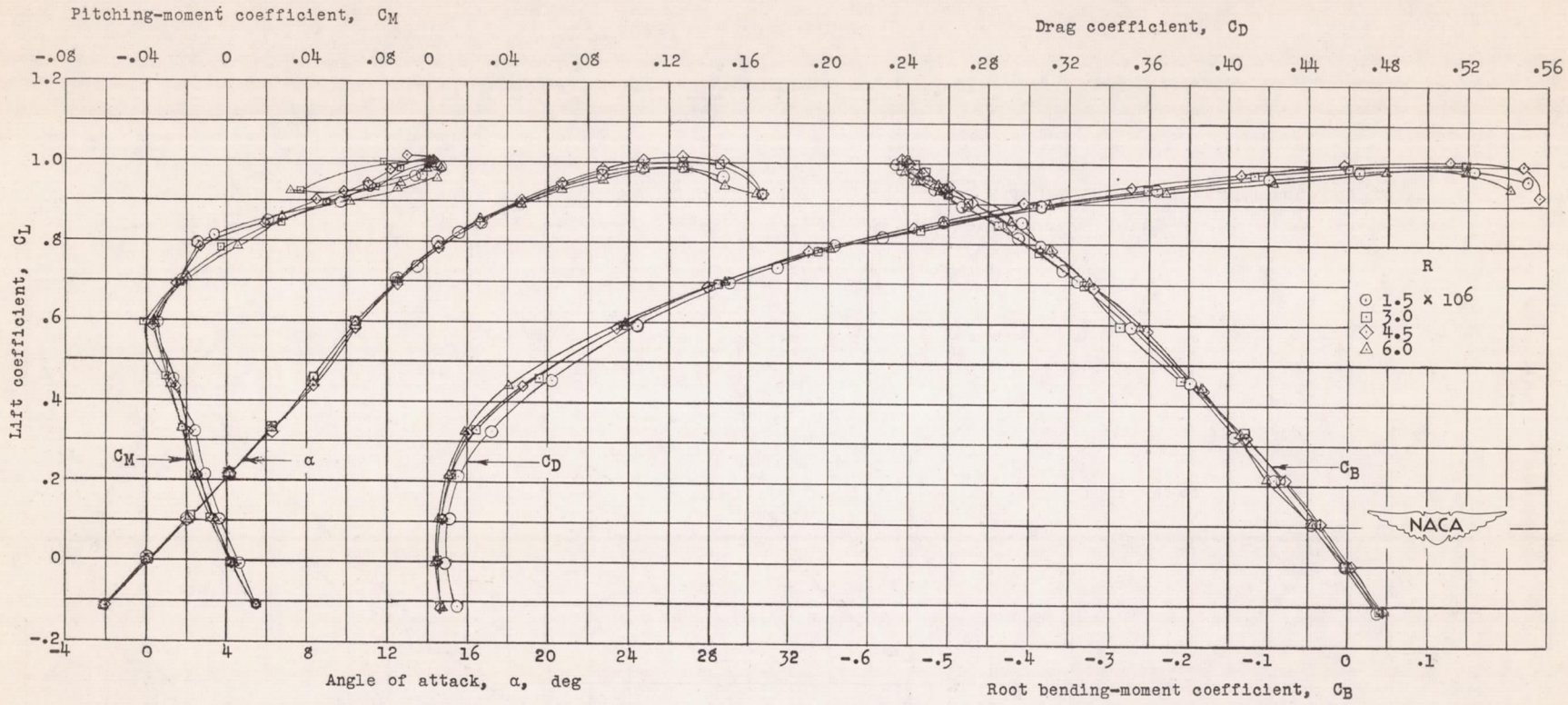

(a) Plain wing, smooth.

Figure 4.- Low-speed aerodynamic data for the -45-4-0.6 wing at various Reynolds numbers.

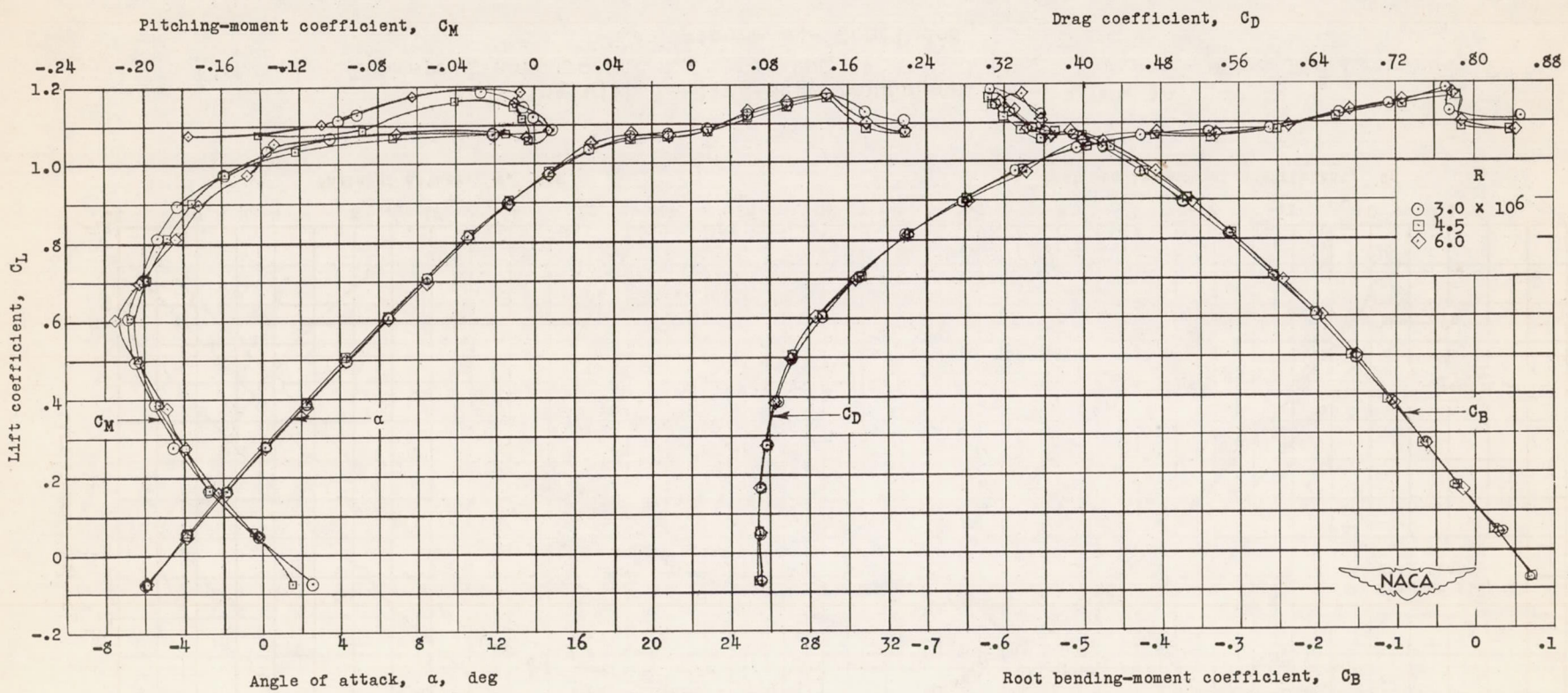

(b) Wing with $0.50\frac{b}{2}$ split flap, smooth.

Figure 4.- Continued.

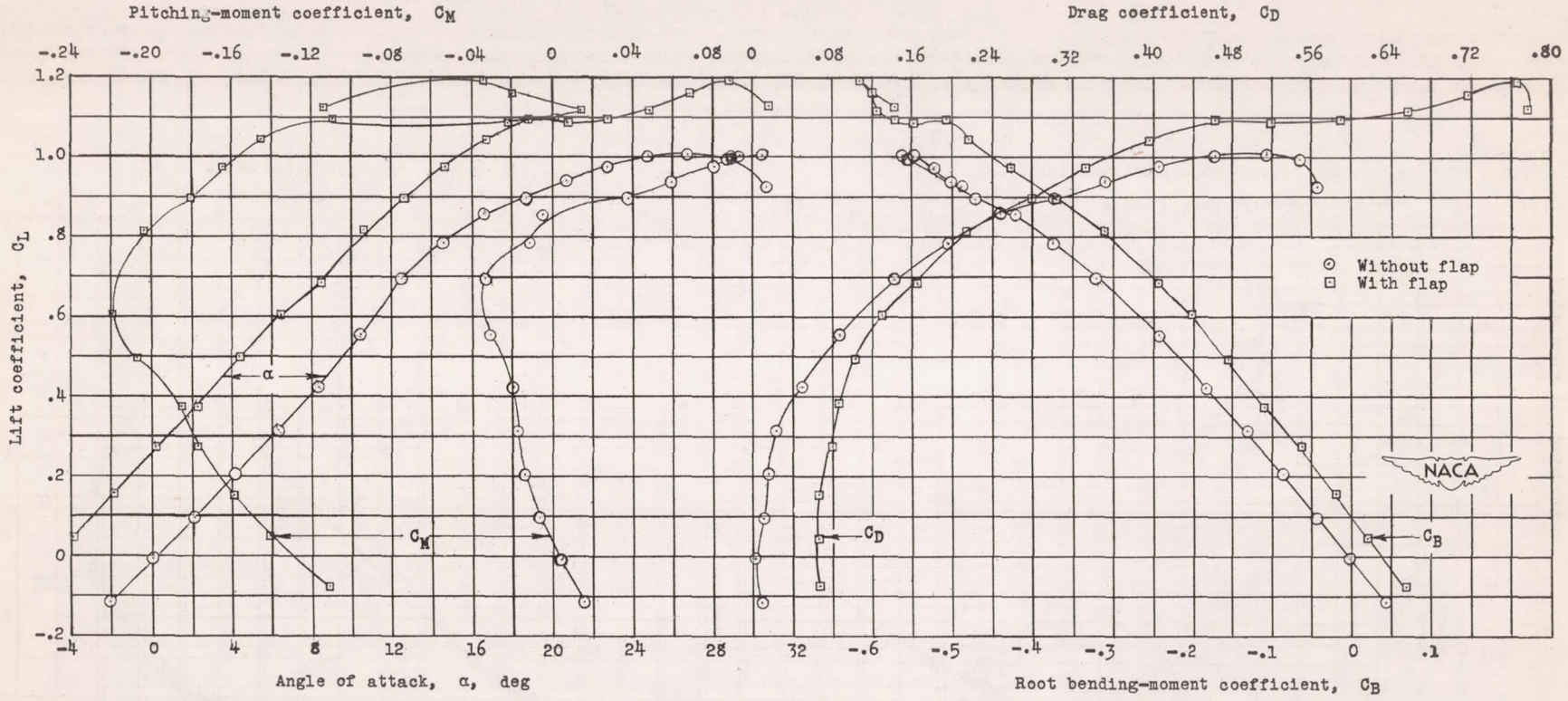

(c) Wing with leading-edge roughness. $R = 3.0 \times 10^6$.

Figure 4.- Concluded.

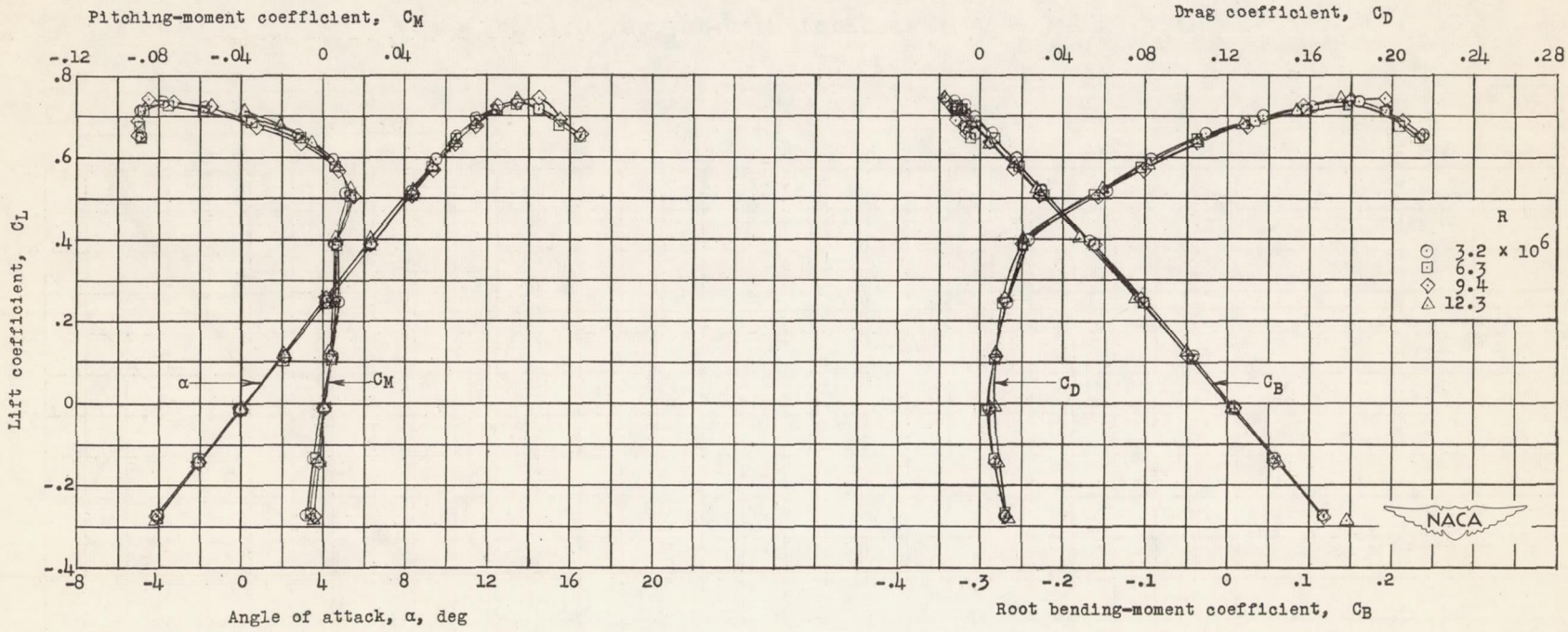

(a) Plain wing, smooth.

Figure 5.- Low-speed aerodynamic data for the 0-4-0.6 wing at various Reynolds numbers.

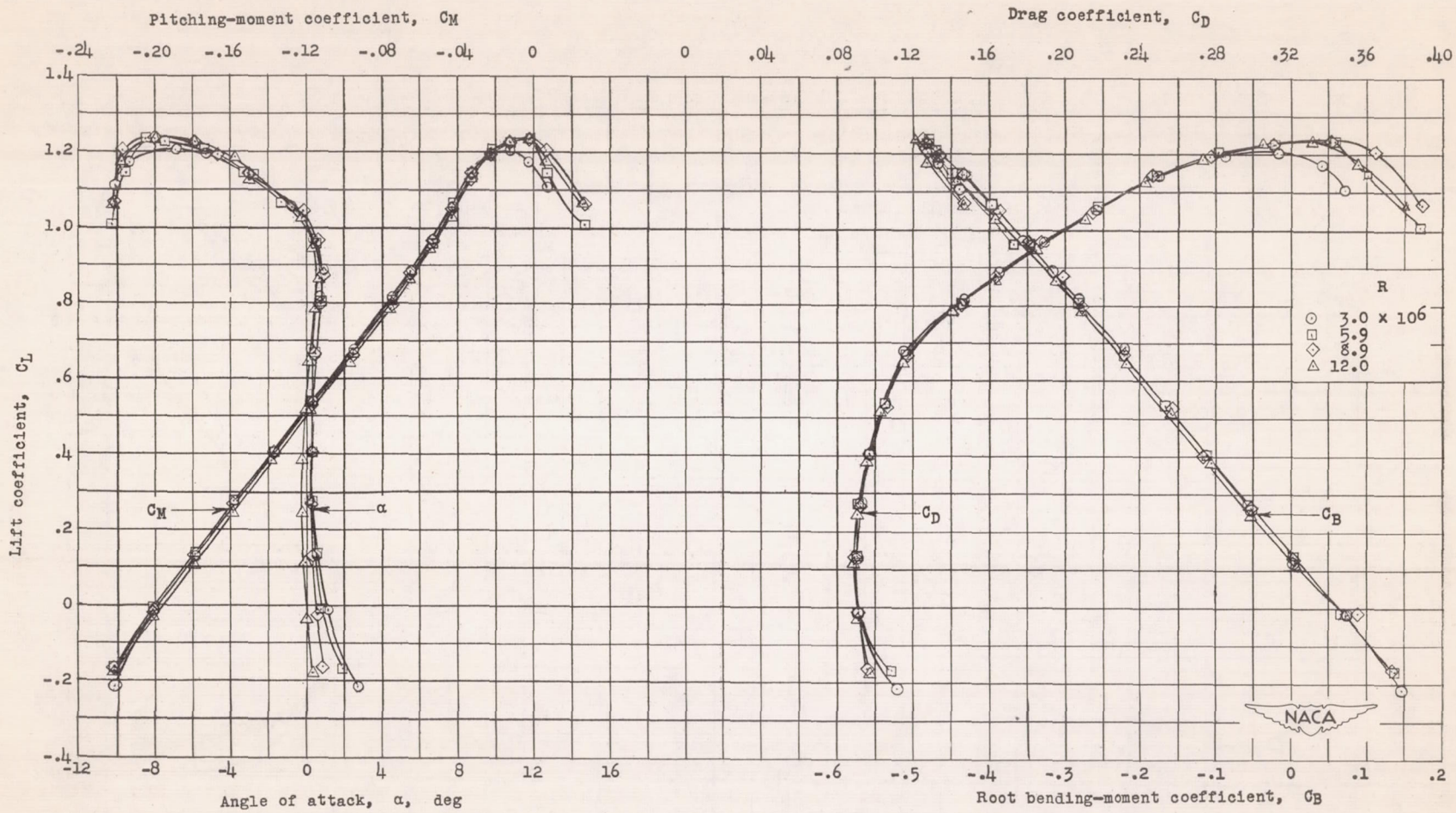

(b) Wing with $0.50\frac{b}{2}$ split flap, smooth.

Figure 5.- Continued.

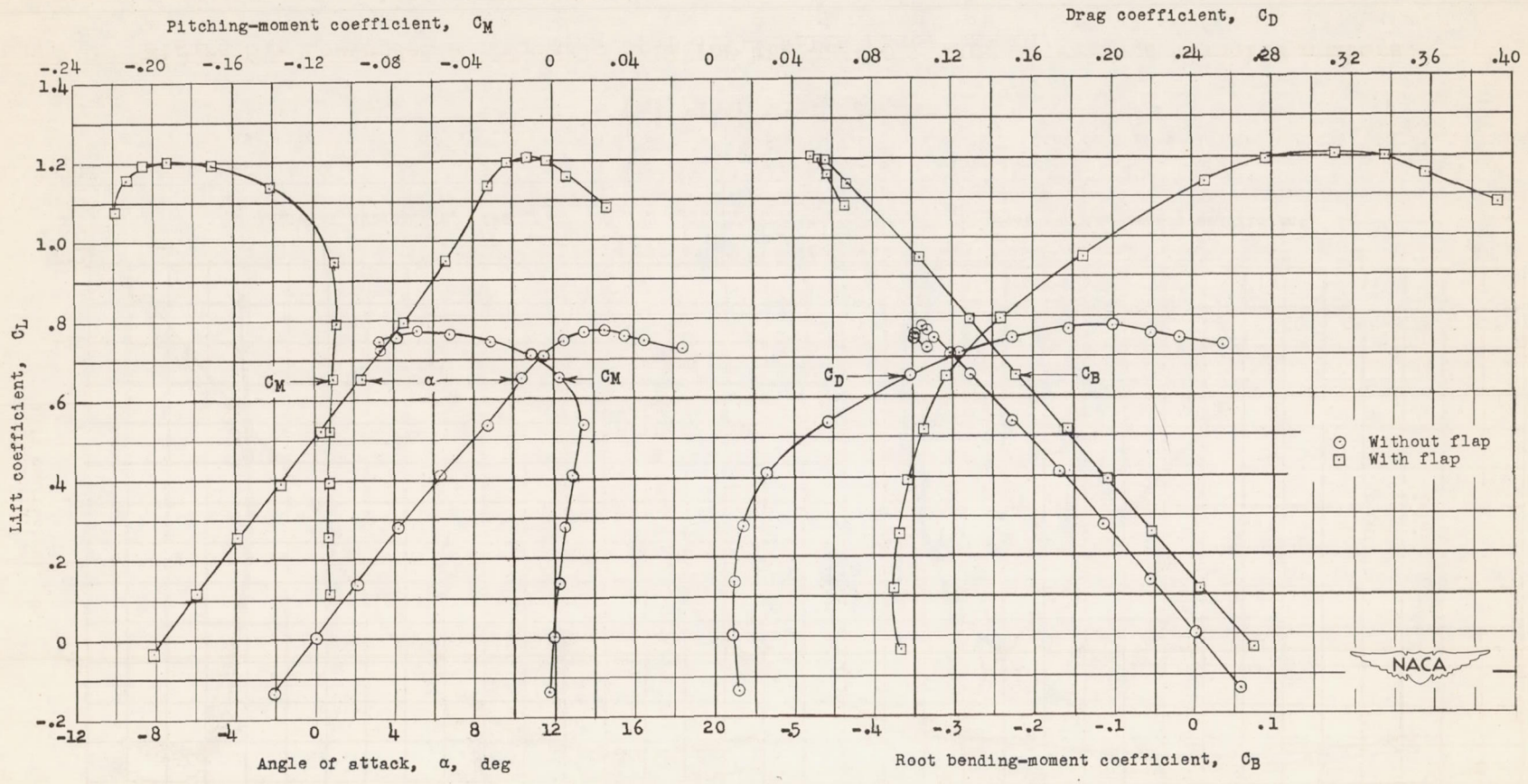

(c) Wing with leading-edge roughness. $R = 5.9 \times 10^6$.

Figure 5.- Concluded.

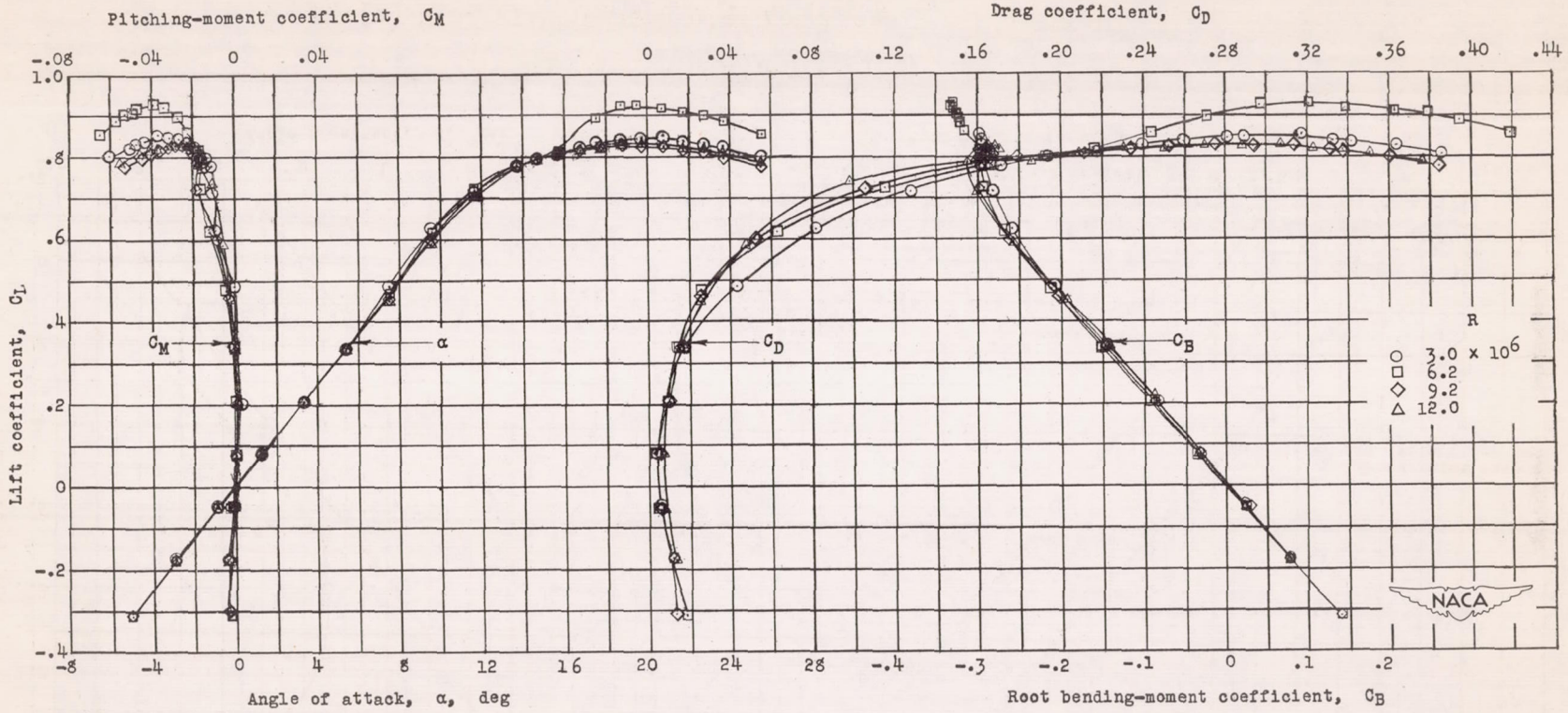

(a) Plain wing, smooth.

Figure 6.- Low-speed aerodynamic data for the 30-4-0.6 wing at various Reynolds numbers.

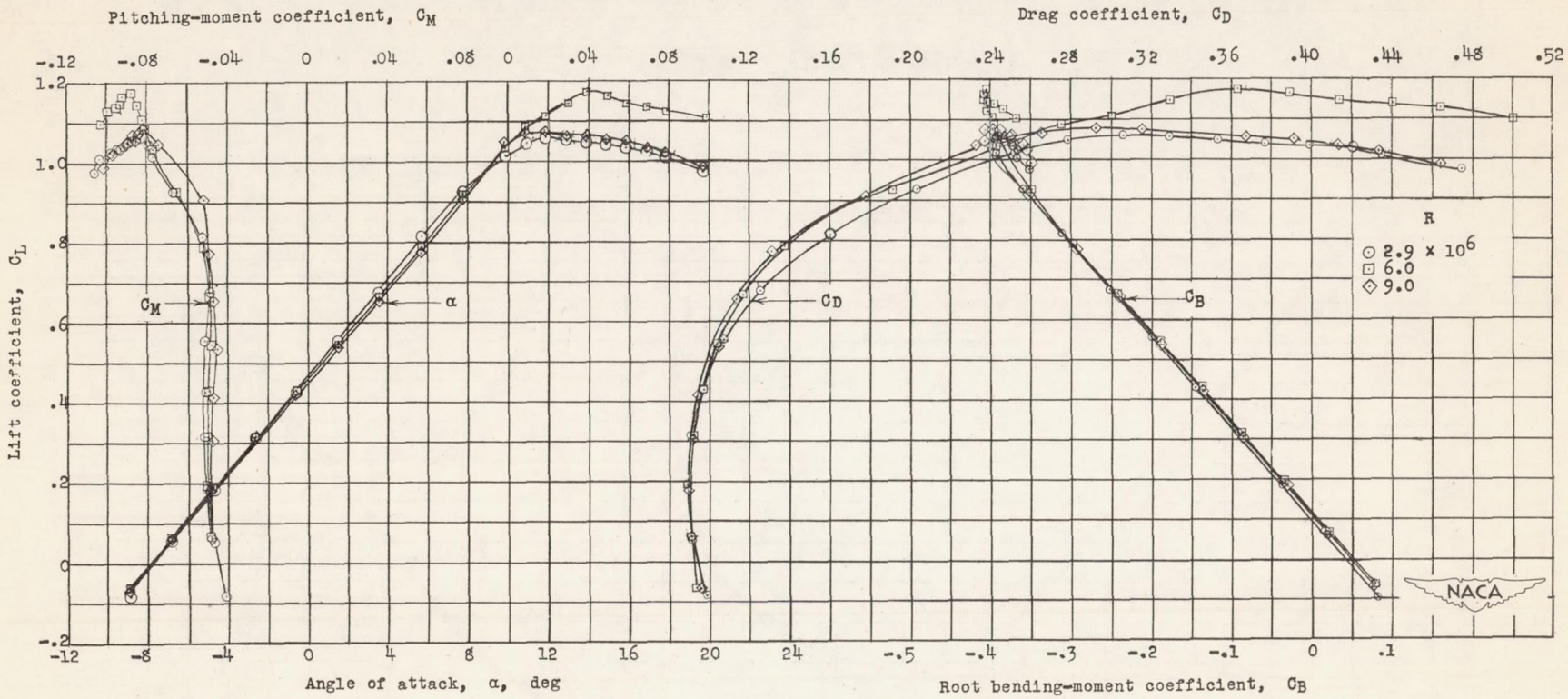

(b) Wing with $0.50\frac{b}{2}$ split flap, smooth.

Figure 6.- Continued.

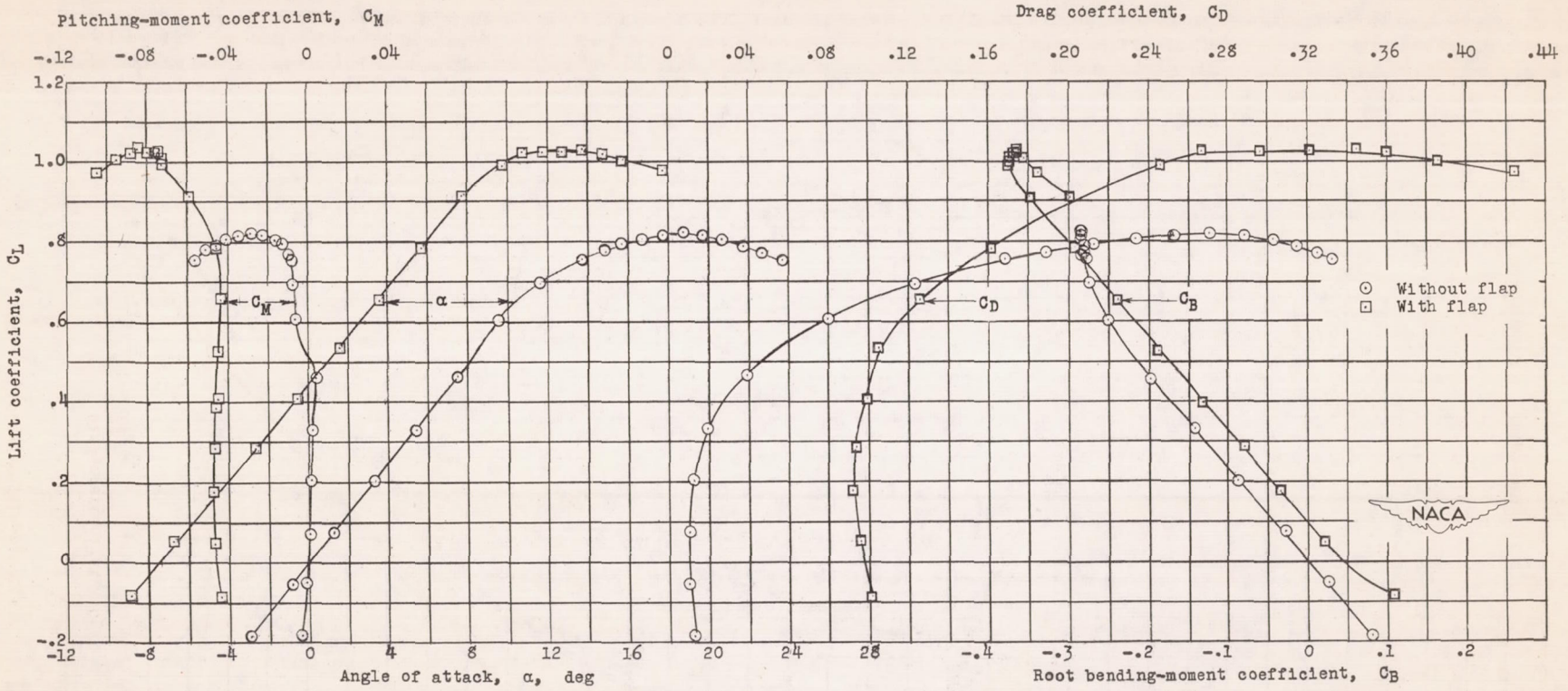

(c) Wing with leading-edge roughness. $R = 5.9 \times 10^6$.

Figure 6.- Concluded.

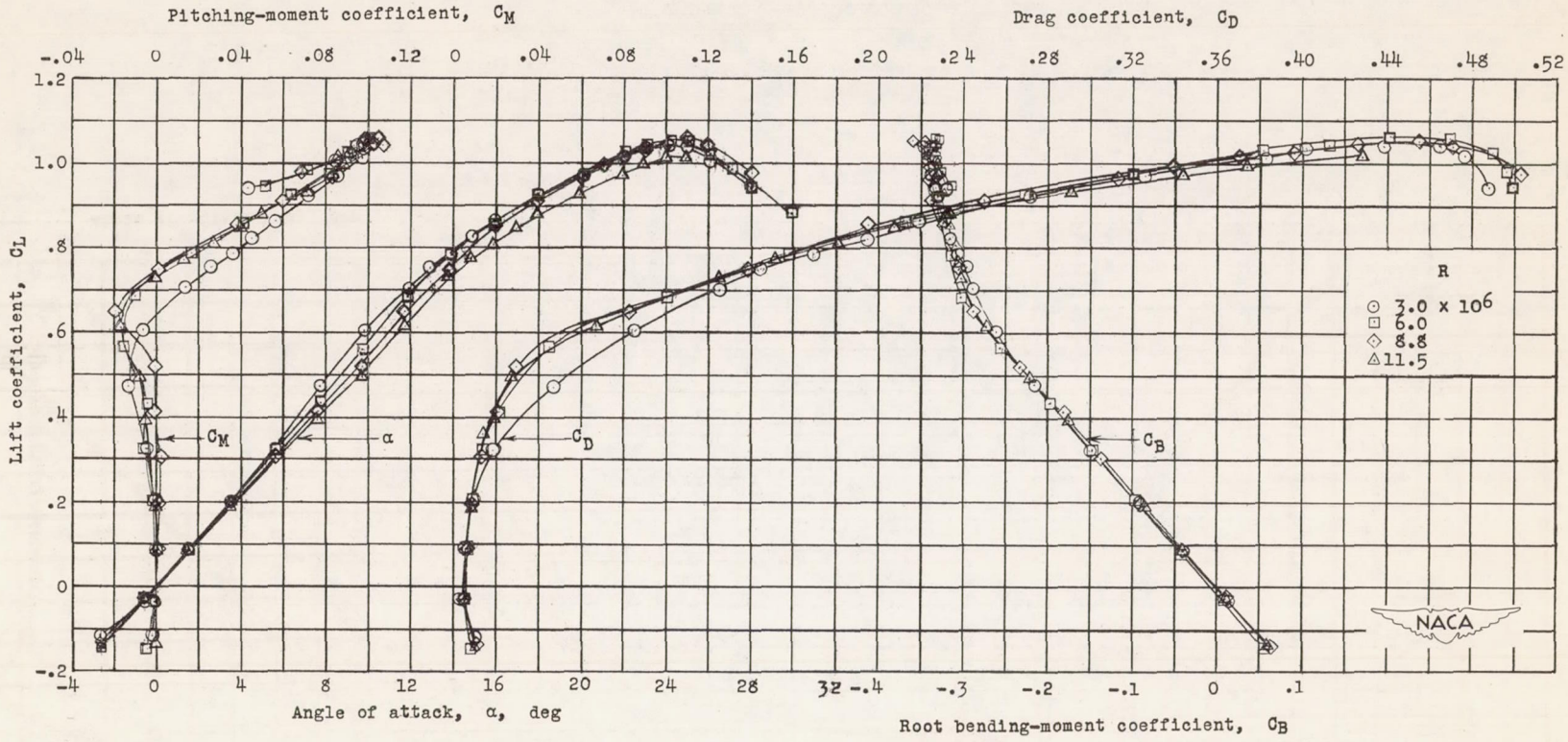

(a) Plain wing, smooth.

Figure 7.- Low-speed aerodynamic data for the 45-4-0.6 wing at various Reynolds numbers.

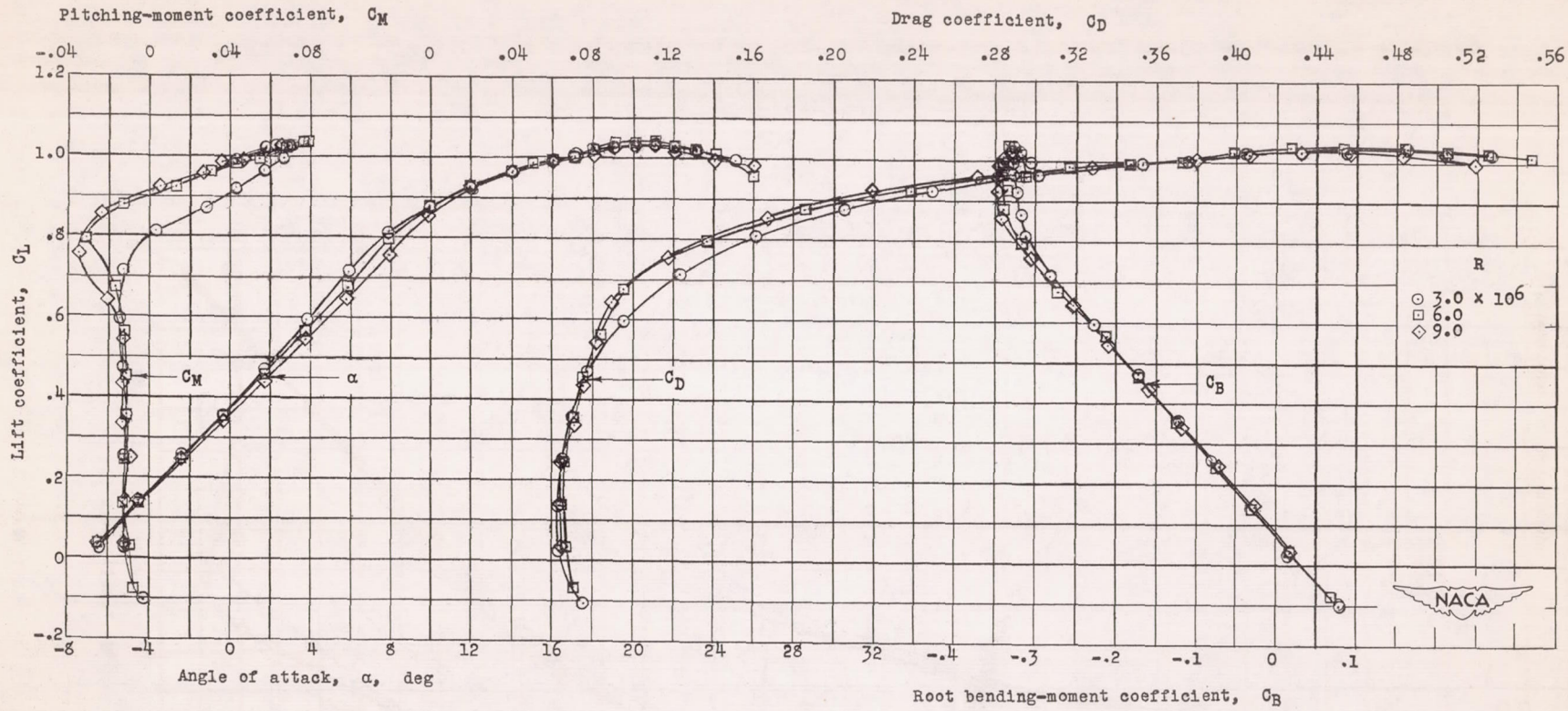

(b) Wing with $0.50\frac{b}{2}$ split flap, smooth.

Figure 7.- Continued.

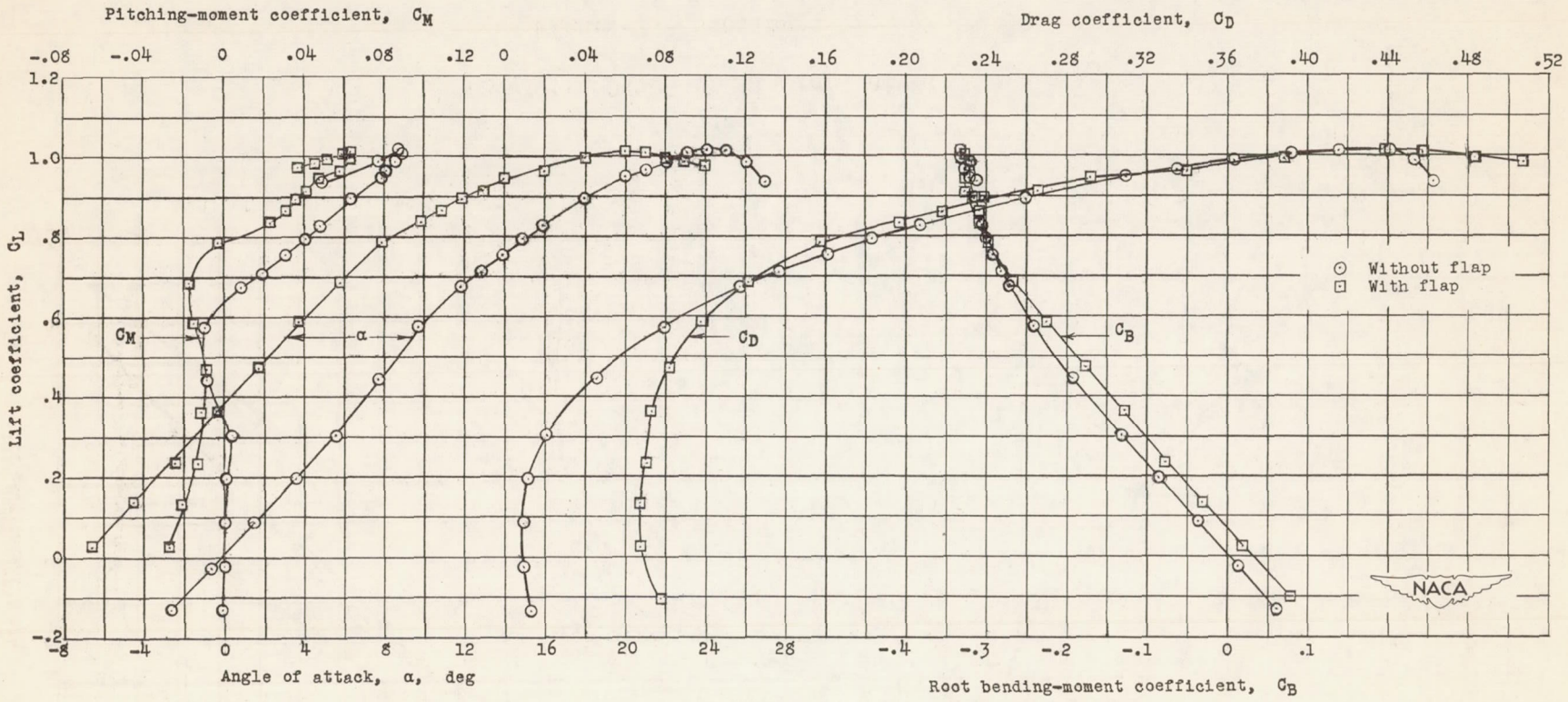

(c) Wing with leading-edge roughness. $R = 6.0 \times 10^6$.

Figure 7.- Concluded.

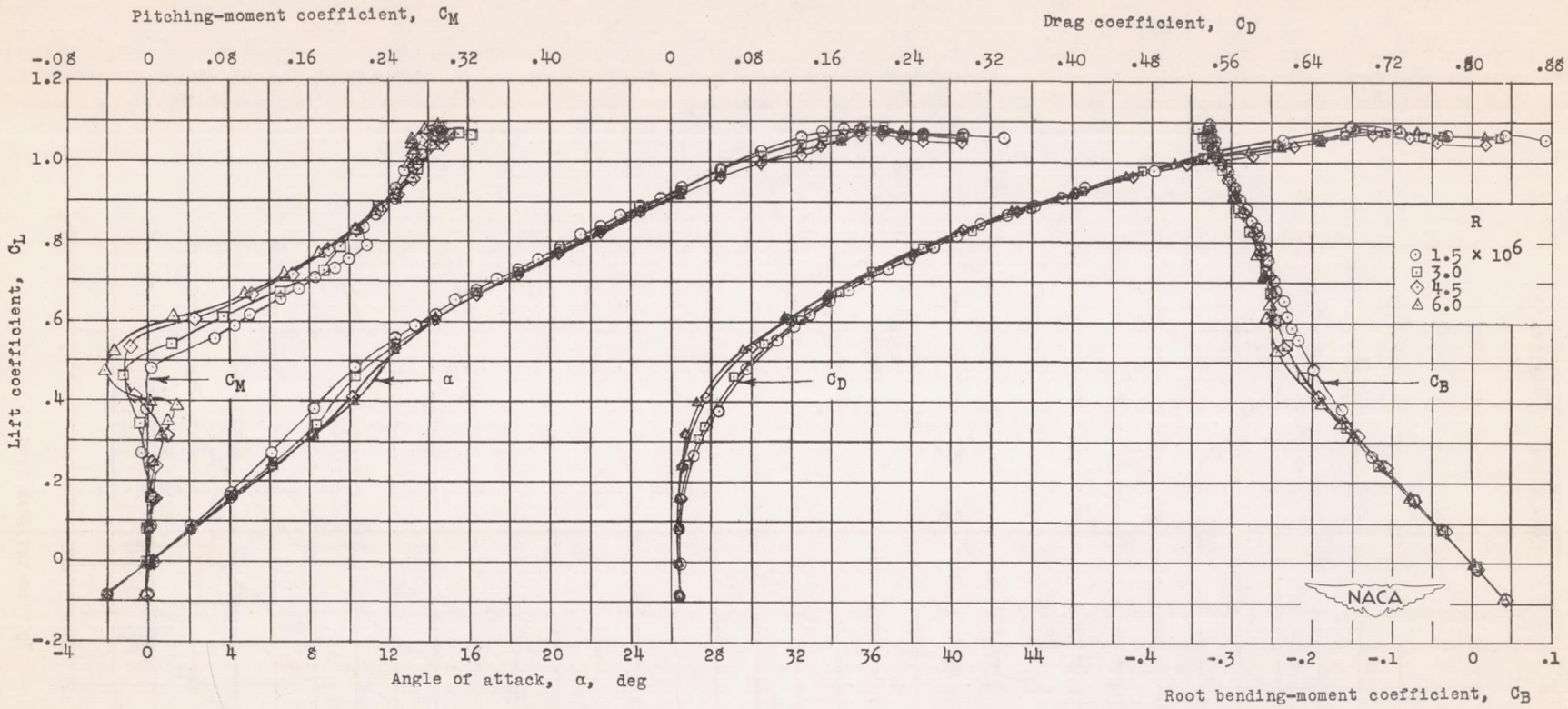

(a) Plain wing, smooth.

Figure 8.- Low-speed aerodynamic data for the 60-4-0.6 wing at various Reynolds numbers.

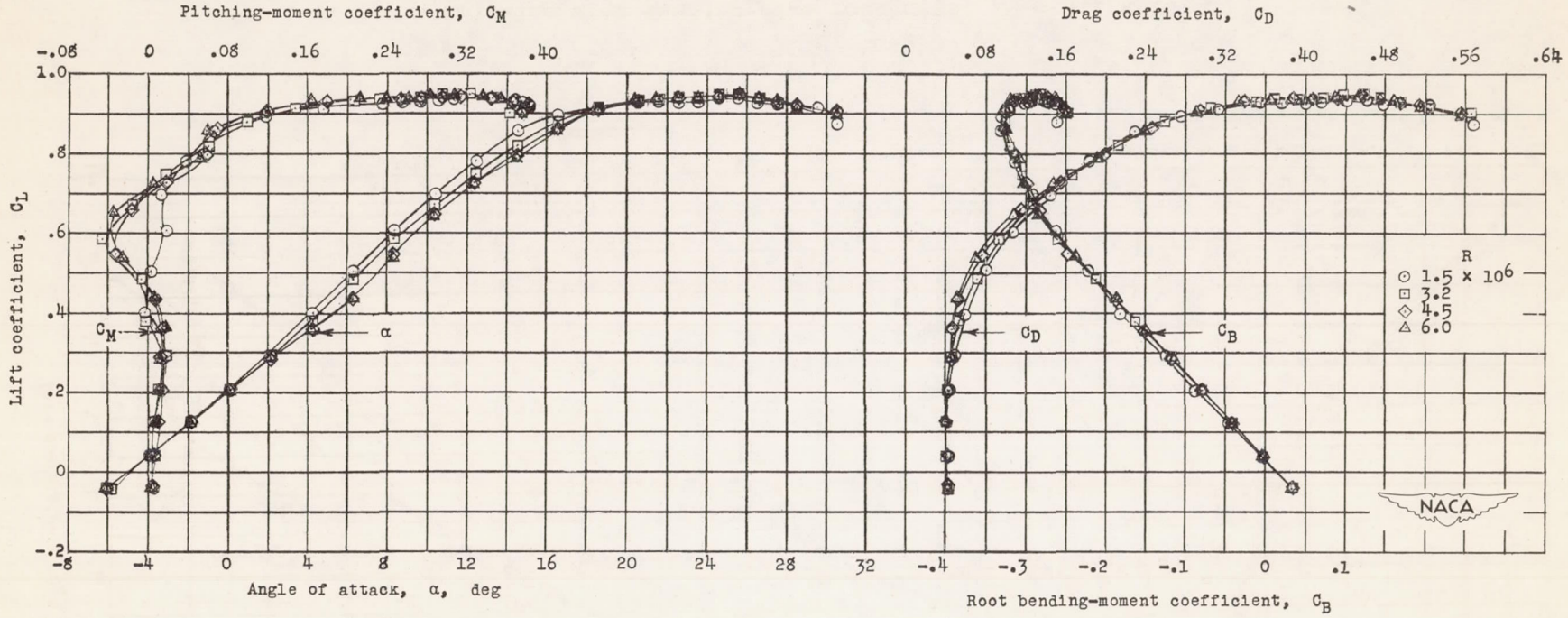

(b) Wing with $0.50\frac{b}{2}$ split flap, smooth.

Figure 8.- Continued.

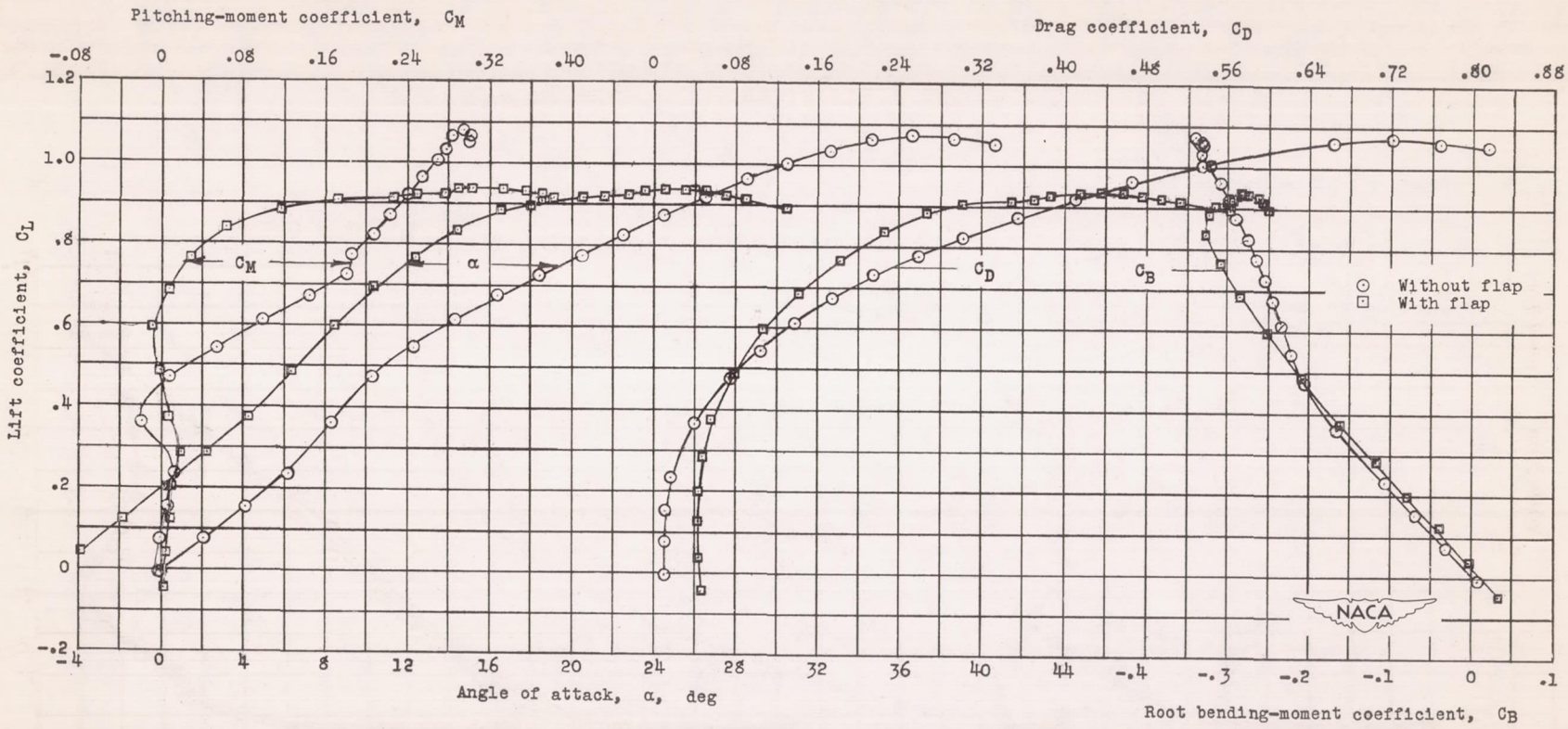

(c) Wing with leading-edge roughness. $R = 3.1 \times 10^6$.

Figure 8.- Concluded.

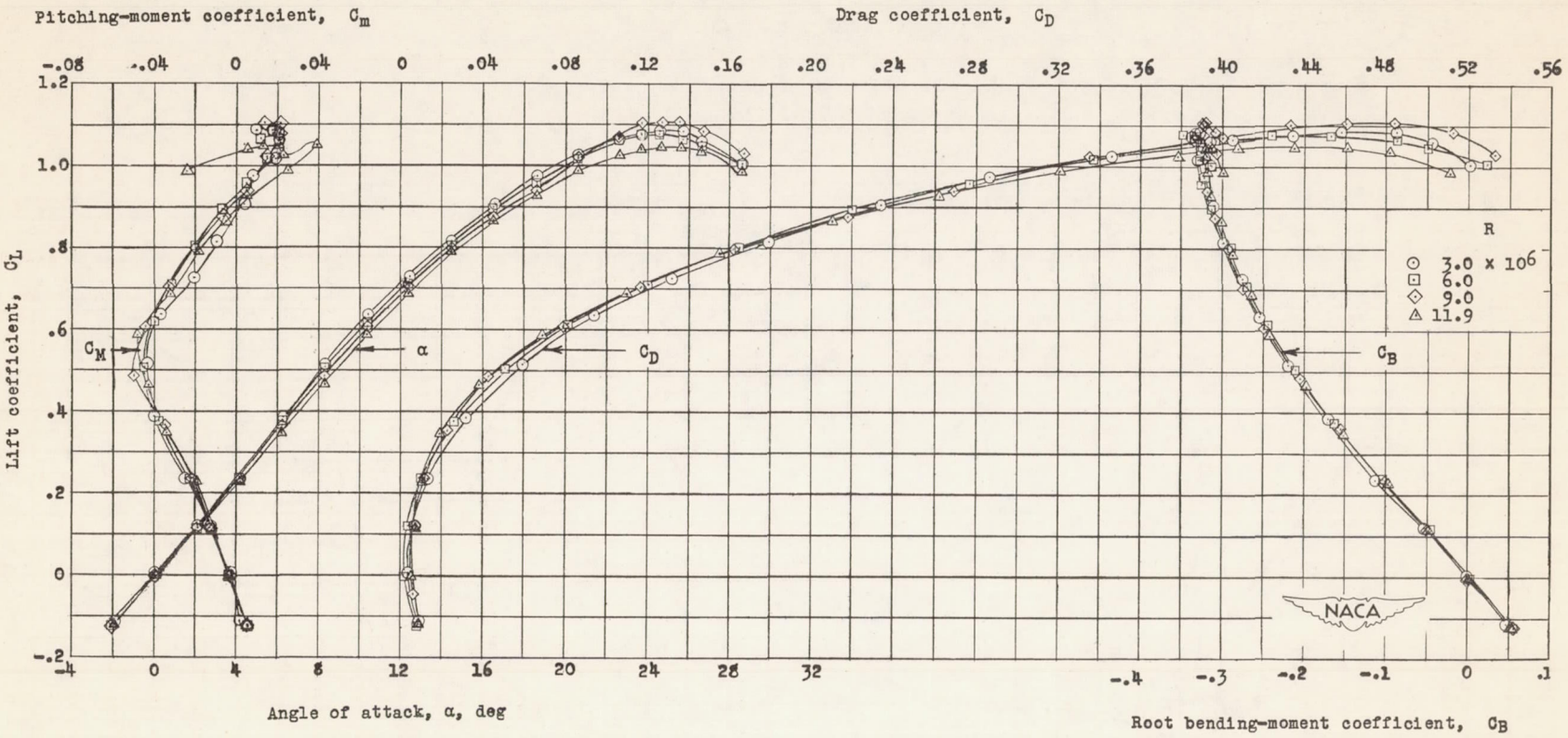

(a) Plain wing, smooth.

Figure 9.- Low-speed aerodynamic data for the 45-4-0.3 wing at various Reynolds numbers.

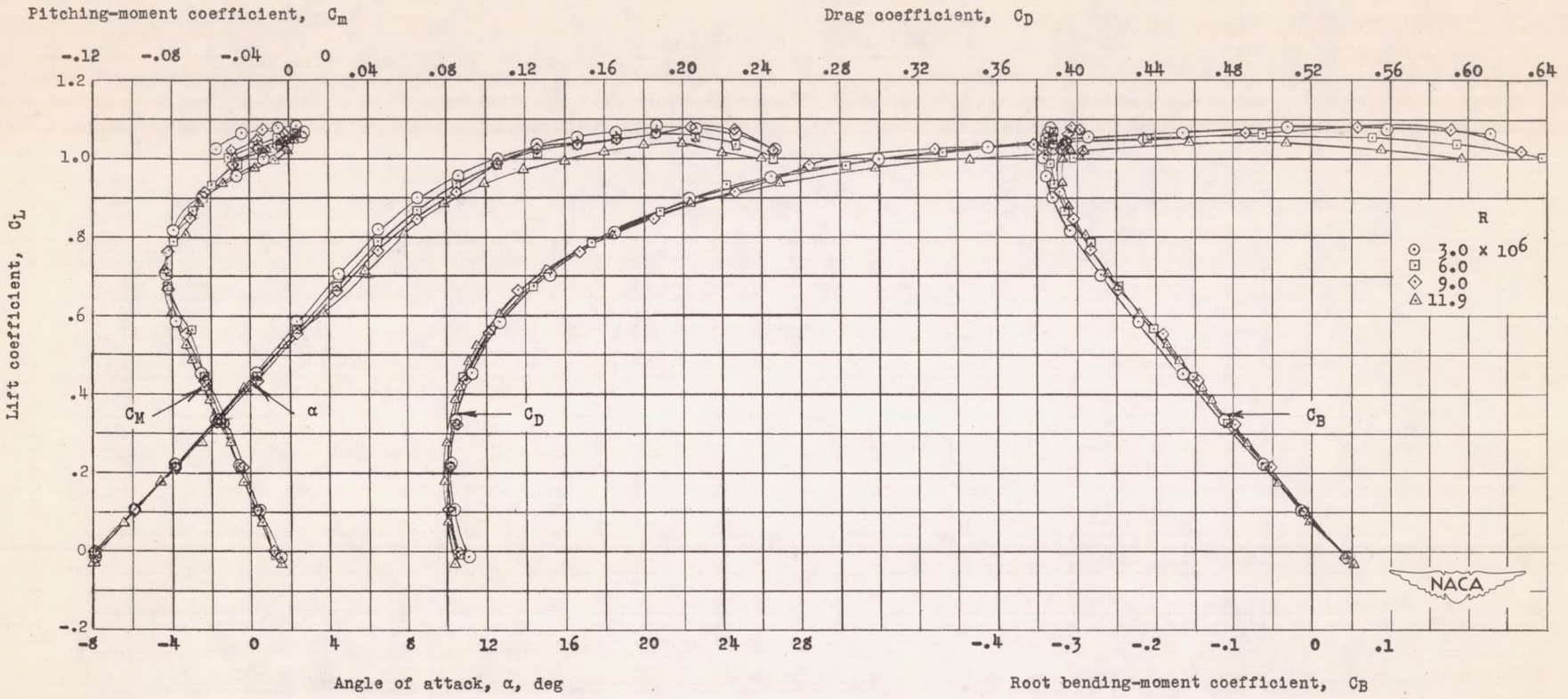

(b) Wing with $0.50\frac{b}{2}$ split flap, smooth.

Figure 9.- Continued.

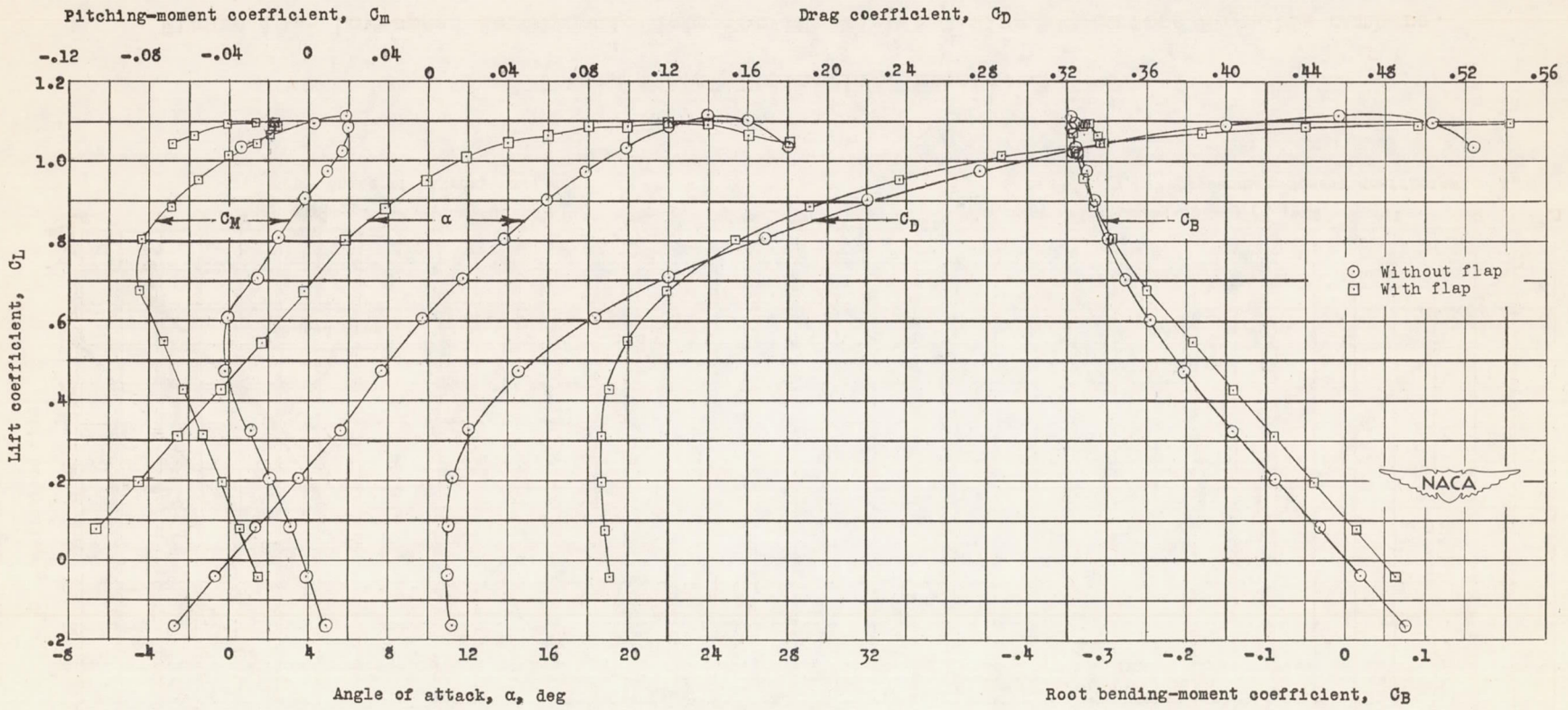

(c) Wing with leading-edge roughness. $R = 3.0 \times 10^6$.

Figure 9.- Concluded.

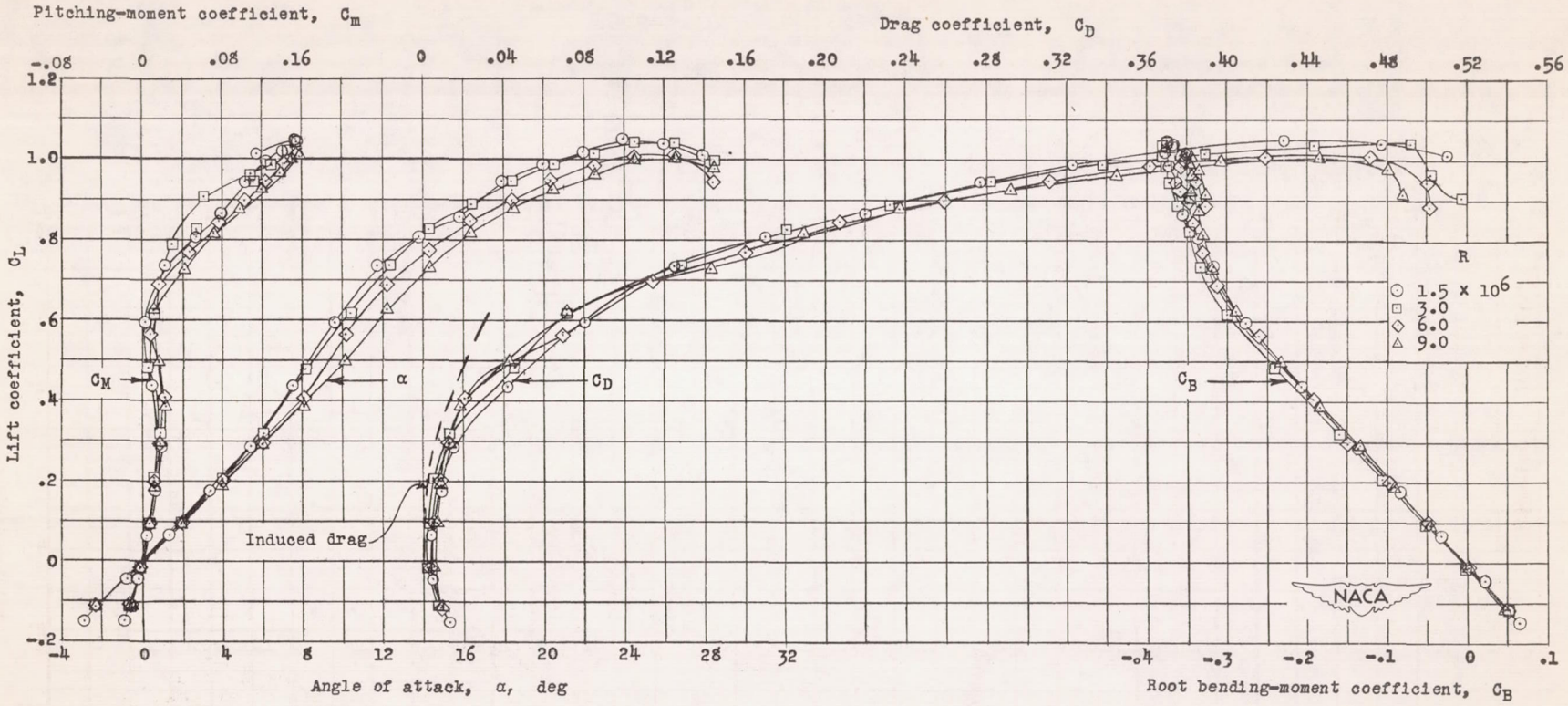

(a) Plain wing, smooth.

Figure 10.- Low-speed aerodynamic data for the 45-4-1.0 wing at various Reynolds numbers.

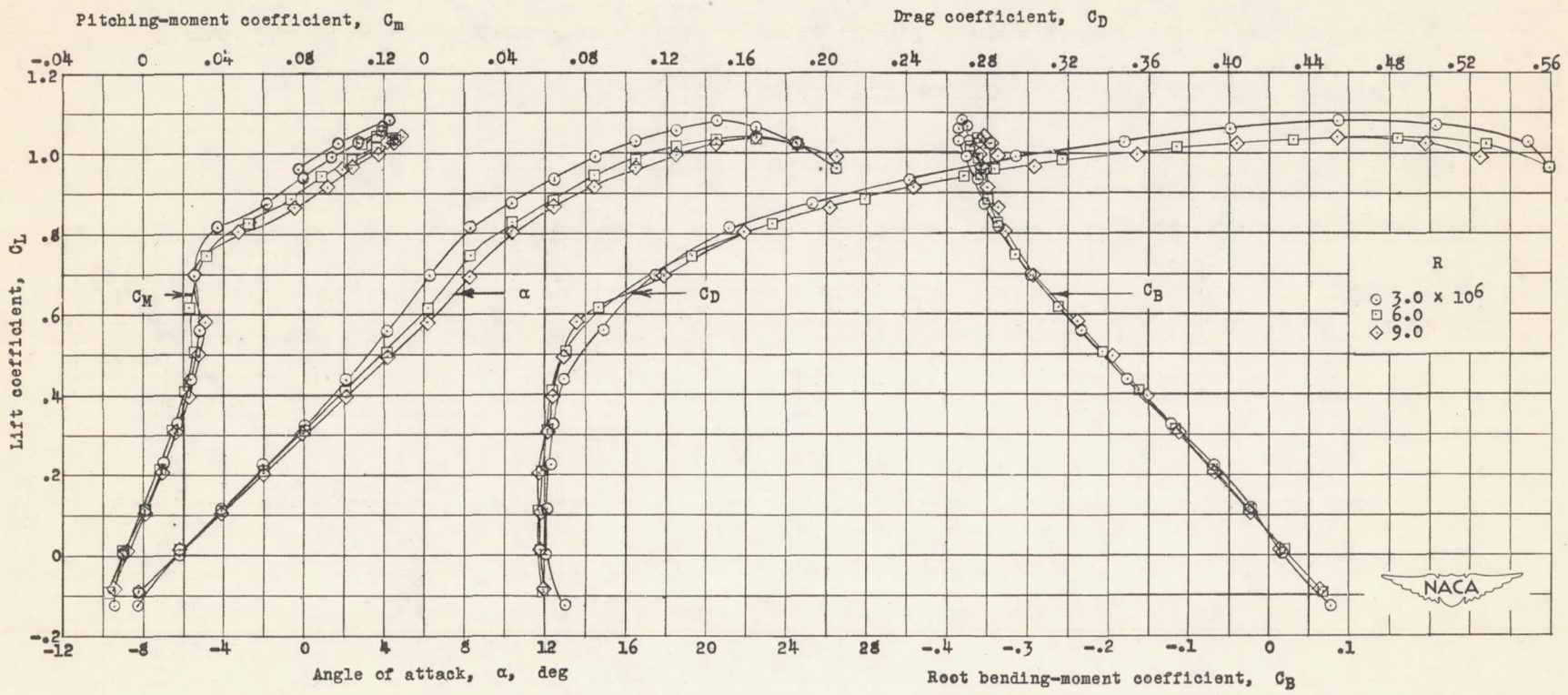

(b) Wing with $0.50\frac{b}{2}$ split flap, smooth.

Figure 10.- Continued.

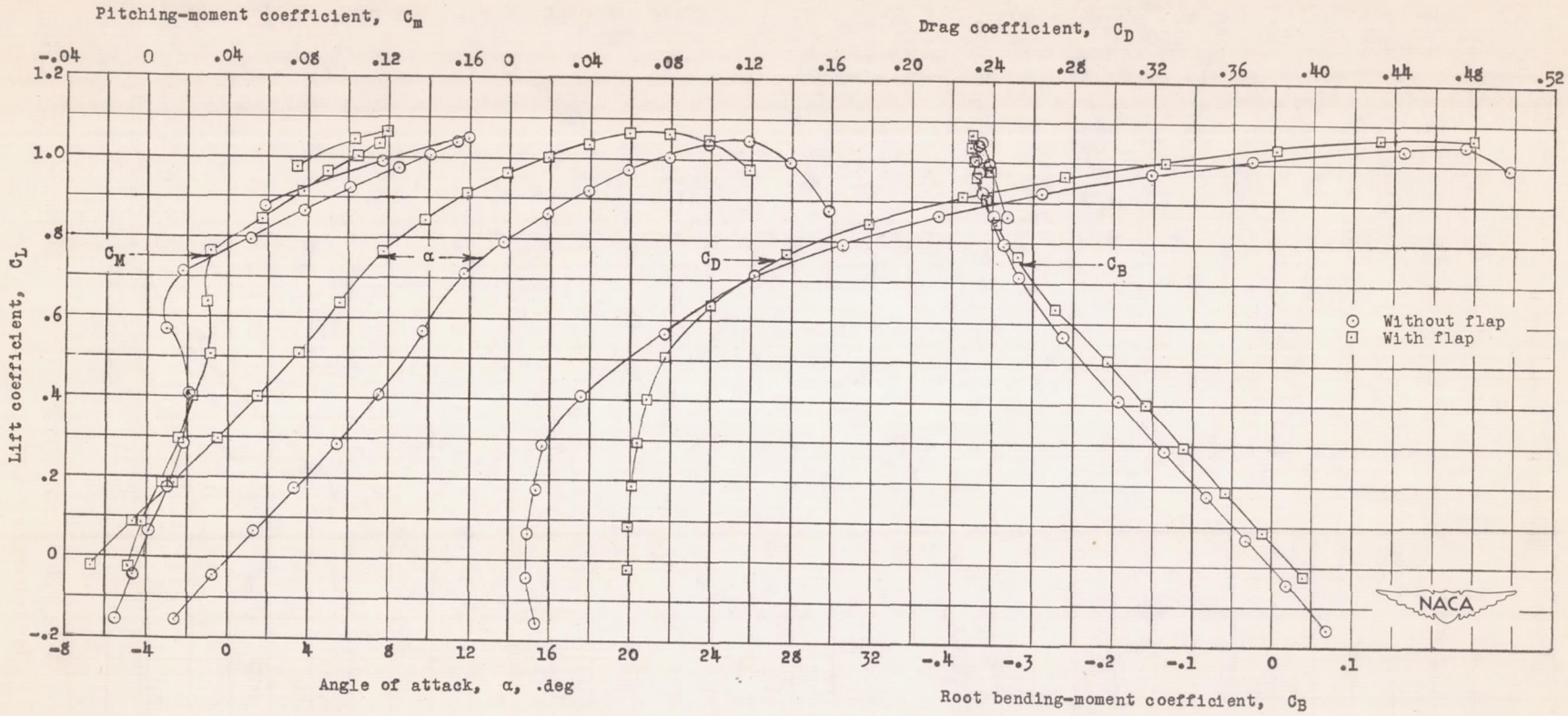

(c) Wing with leading-edge roughness. $R = 3.0 \times 10^6$.

Figure 10.- Concluded.

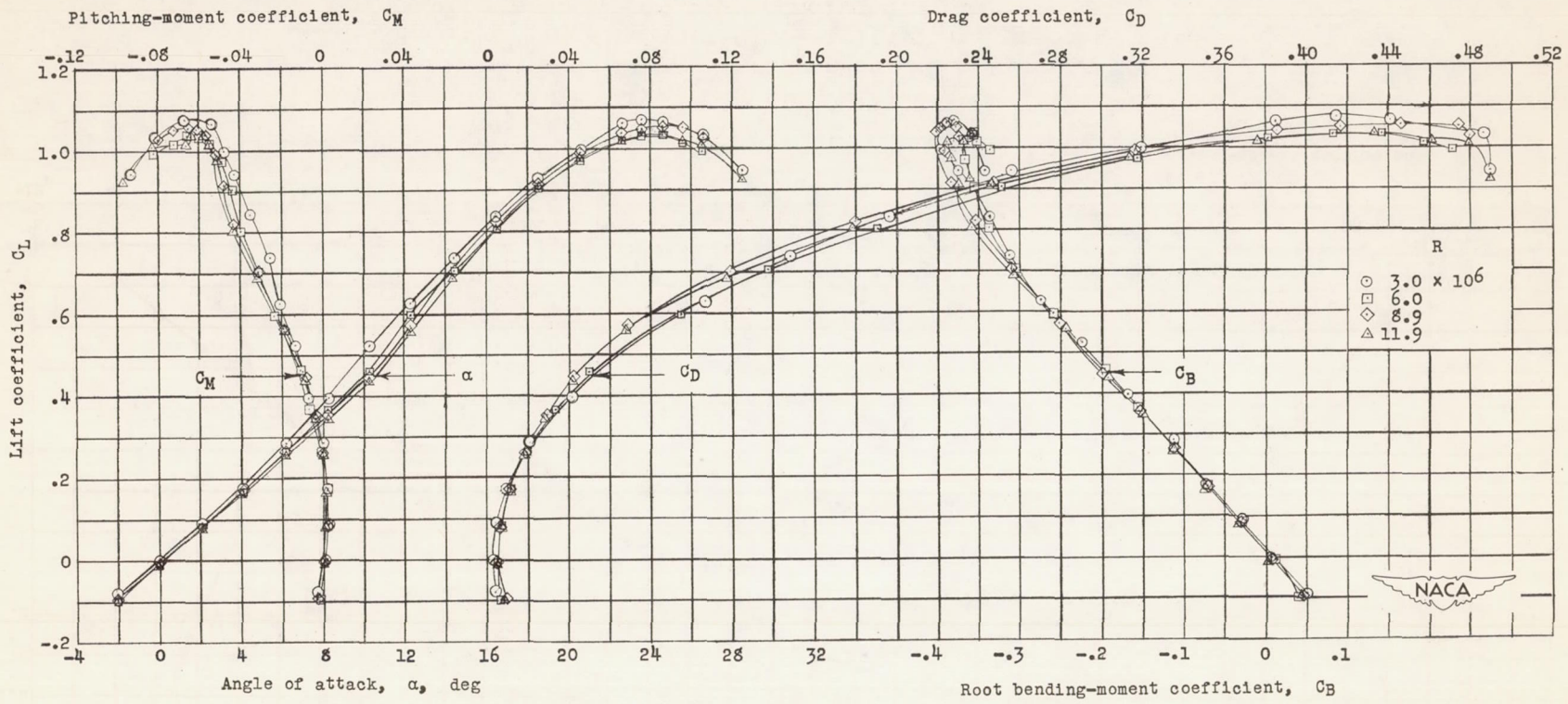

(a) Plain wing, smooth.

Figure 11.- Low-speed aerodynamic data for the 45-2-0.6 wing at various Reynolds numbers.

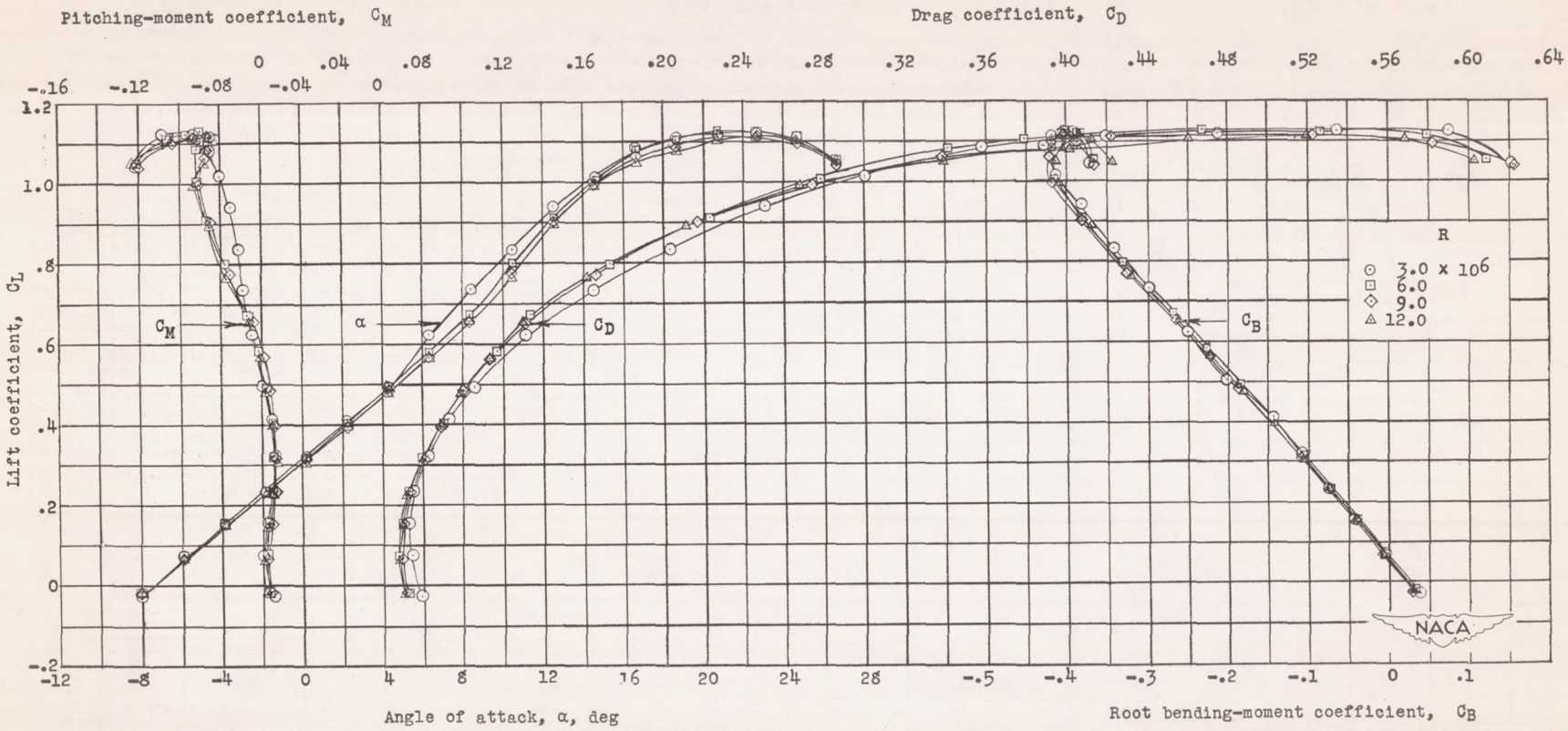

(b) Wing with $0.50\frac{b}{2}$ split flap, smooth.

Figure 11.- Continued.

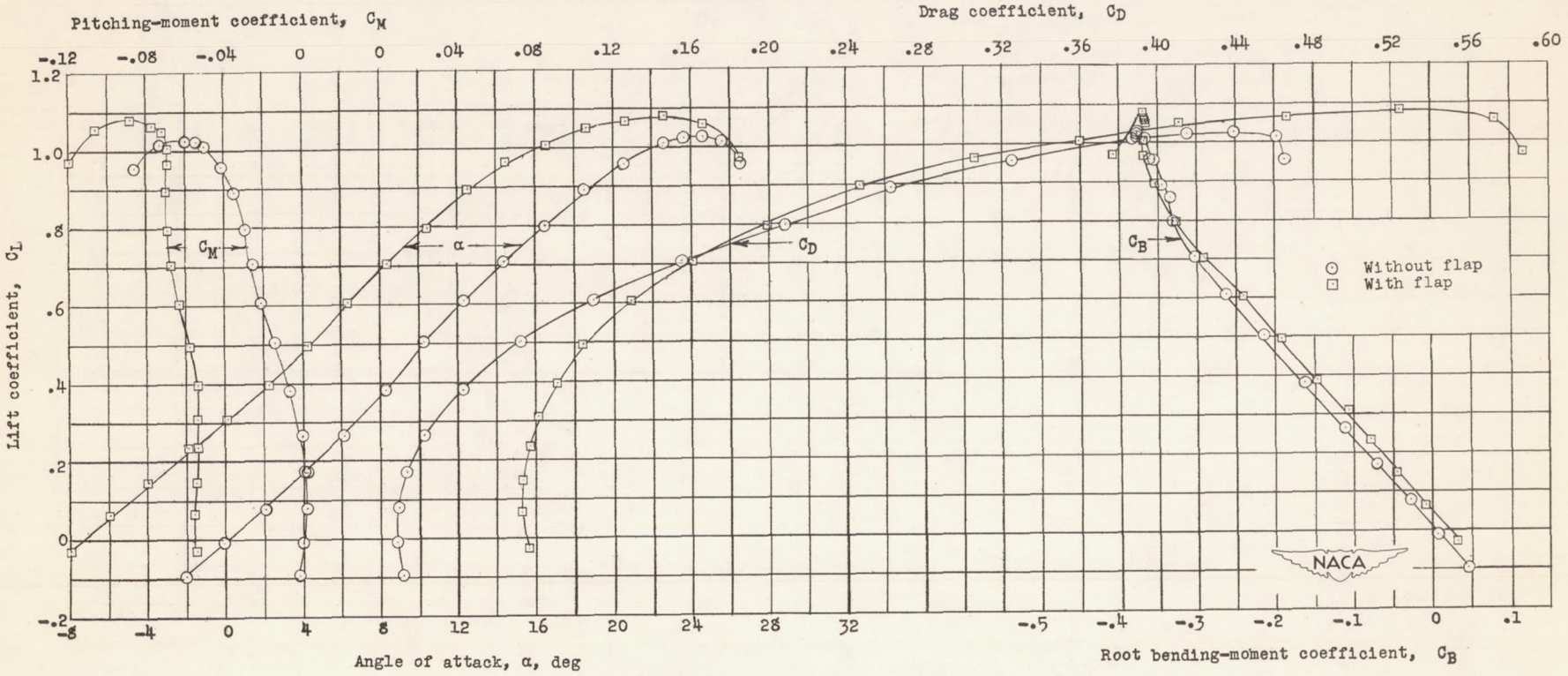

(c) Wing with leading-edge roughness. $R = 6.0 \times 10^6$.

Figure 11.- Concluded.

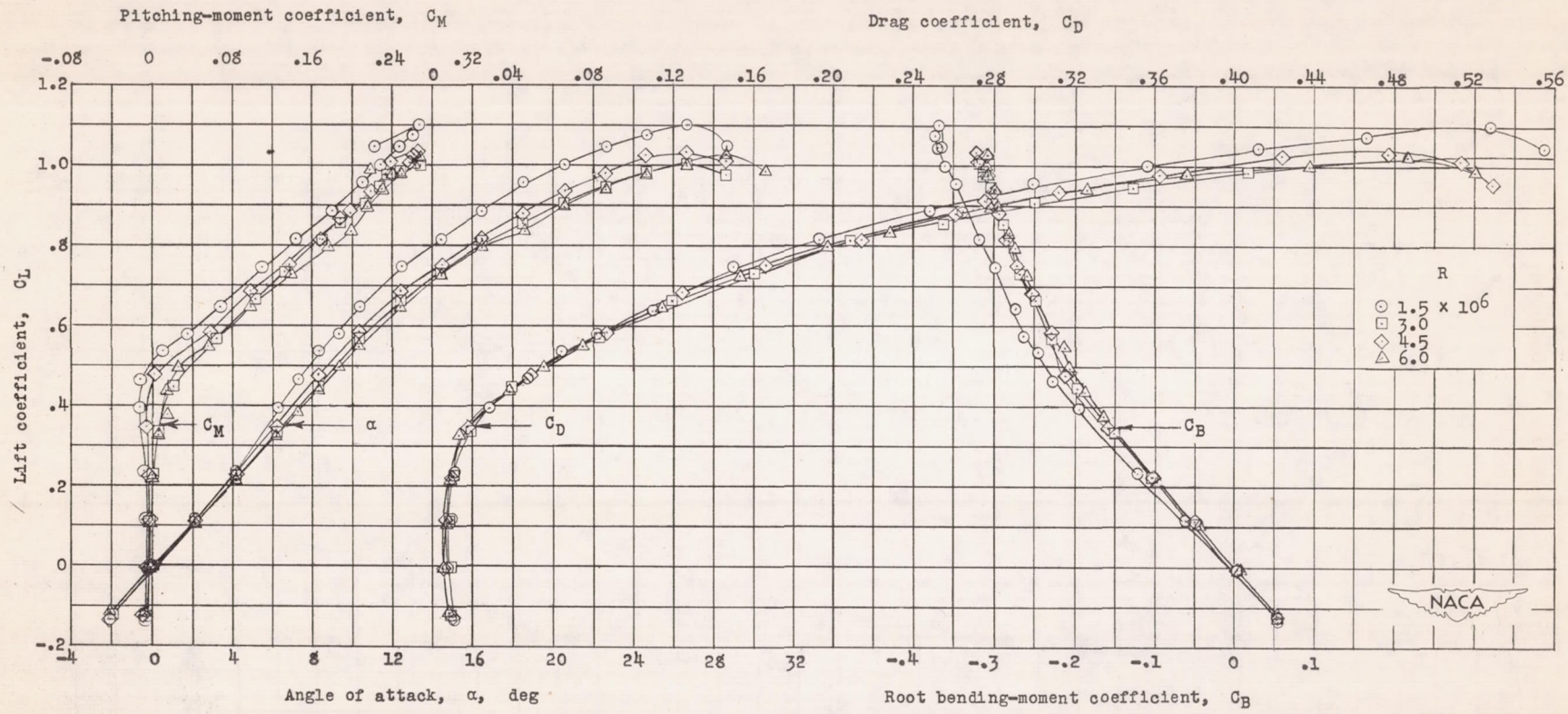

(a) Plain wing, smooth.

Figure 12.- Low-speed aerodynamic data for the 45-6-0.6 wing at various Reynolds numbers.

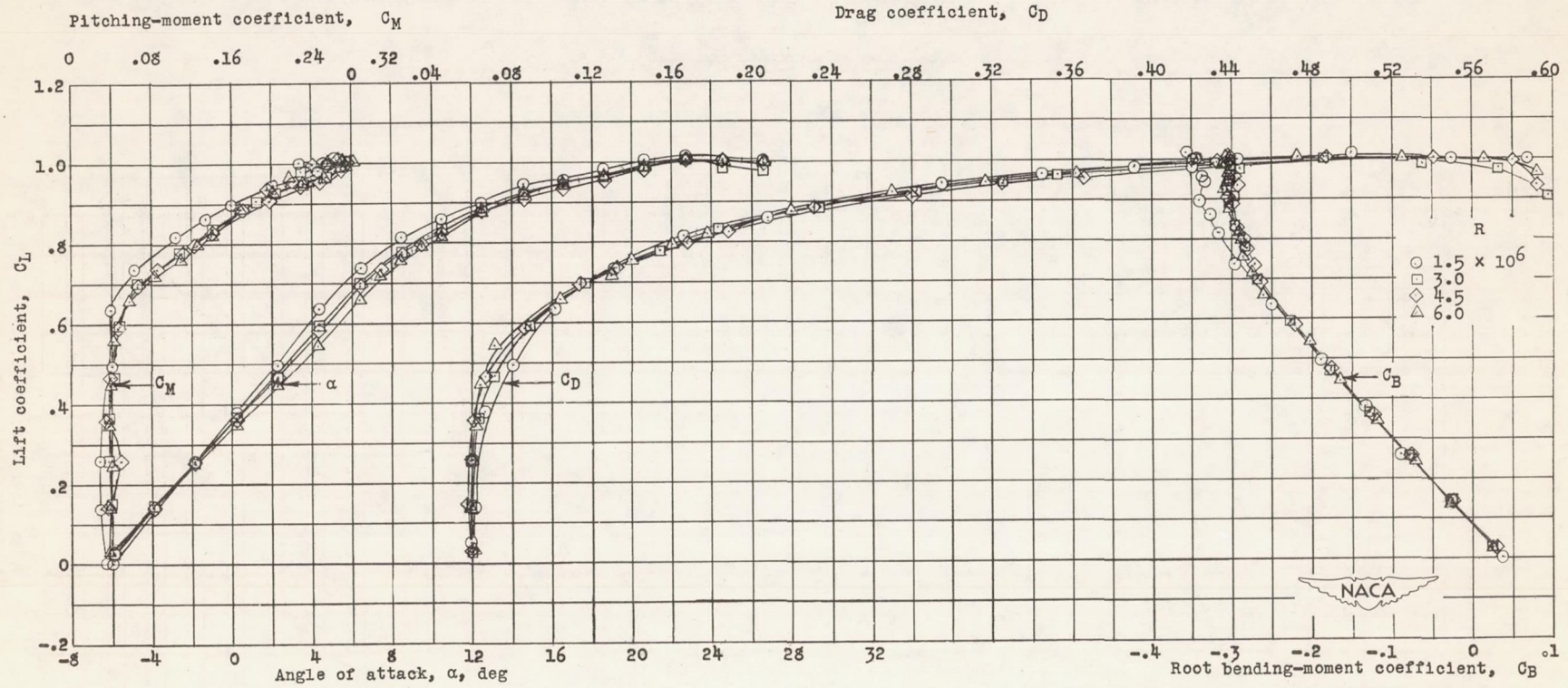

(b) Wing with $0.50\frac{b}{2}$ split flap, smooth.

Figure 12.- Continued.

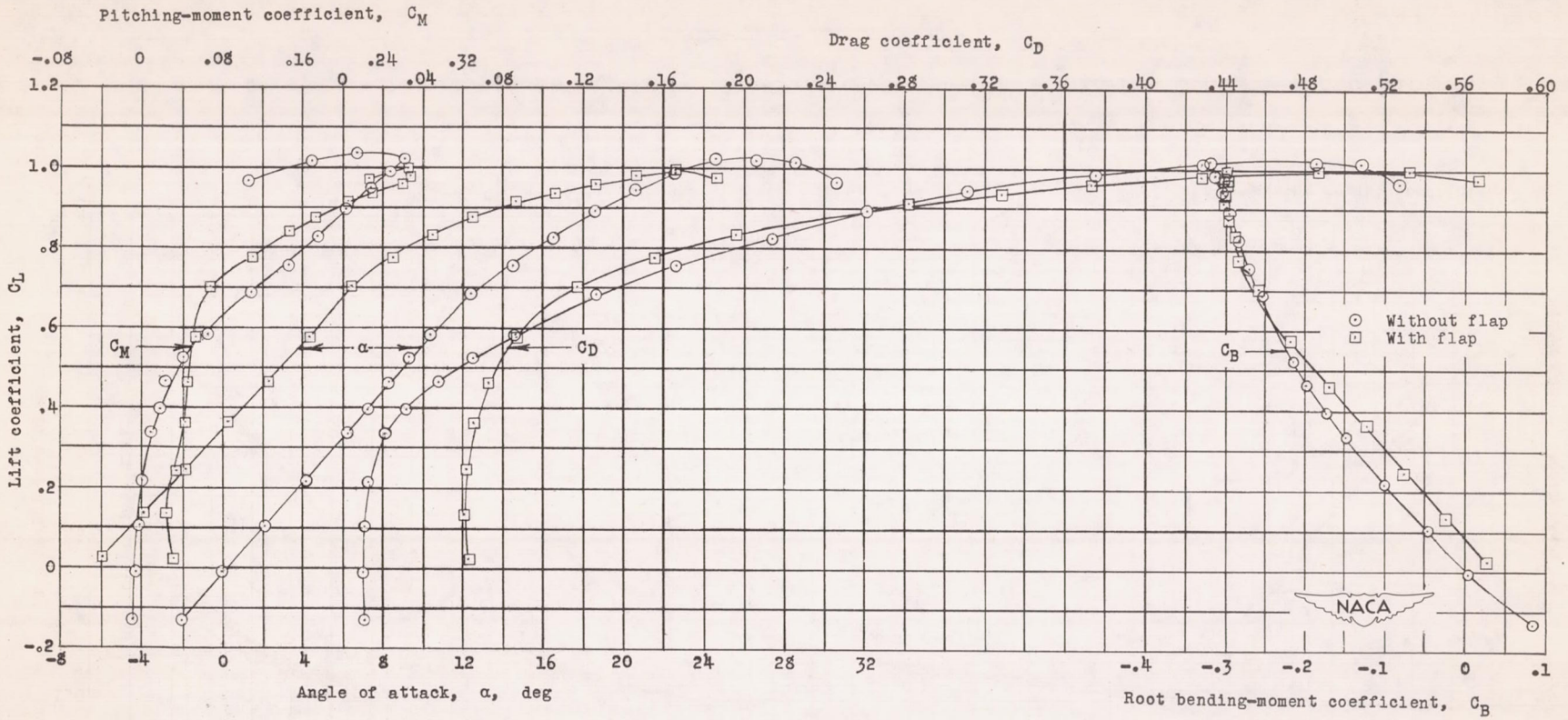

(c) Wing with leading-edge roughness. $R = 3.0 \times 10^6$.

Figure 12.- Concluded.

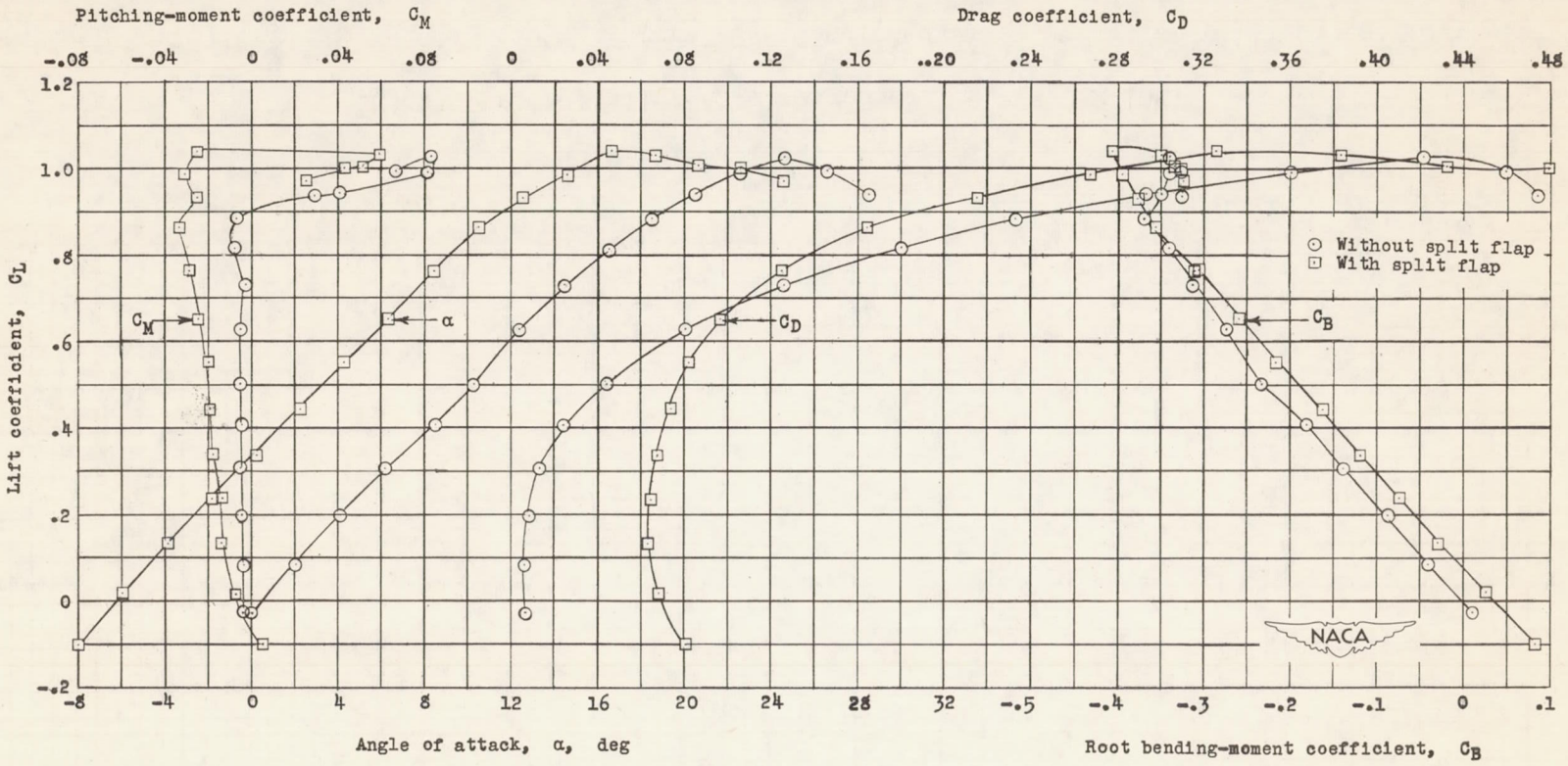

Figure 13.- Low-speed aerodynamic data for the 45-4-0.6 wing with $0.50\frac{b}{2}$ leading-edge flap deflected 10°. $R = 4.5 \times 10^6$.

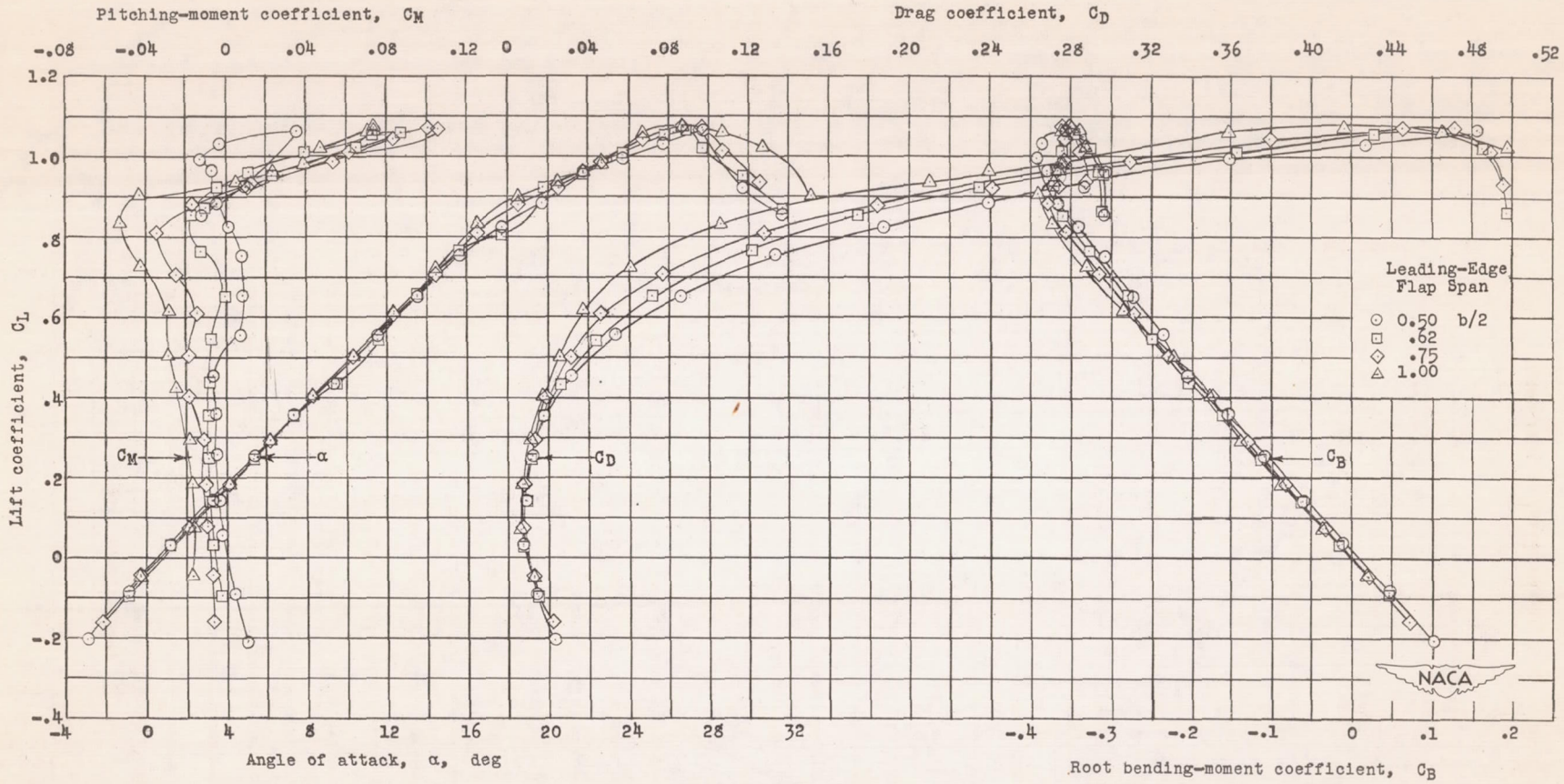

(a) Plain wing, smooth.

Figure 14.- Low-speed aerodynamic data for the 45-4-0.6 wing with leading-edge flaps of various spans deflected 20°. $R = 4.5 \times 10^6$.

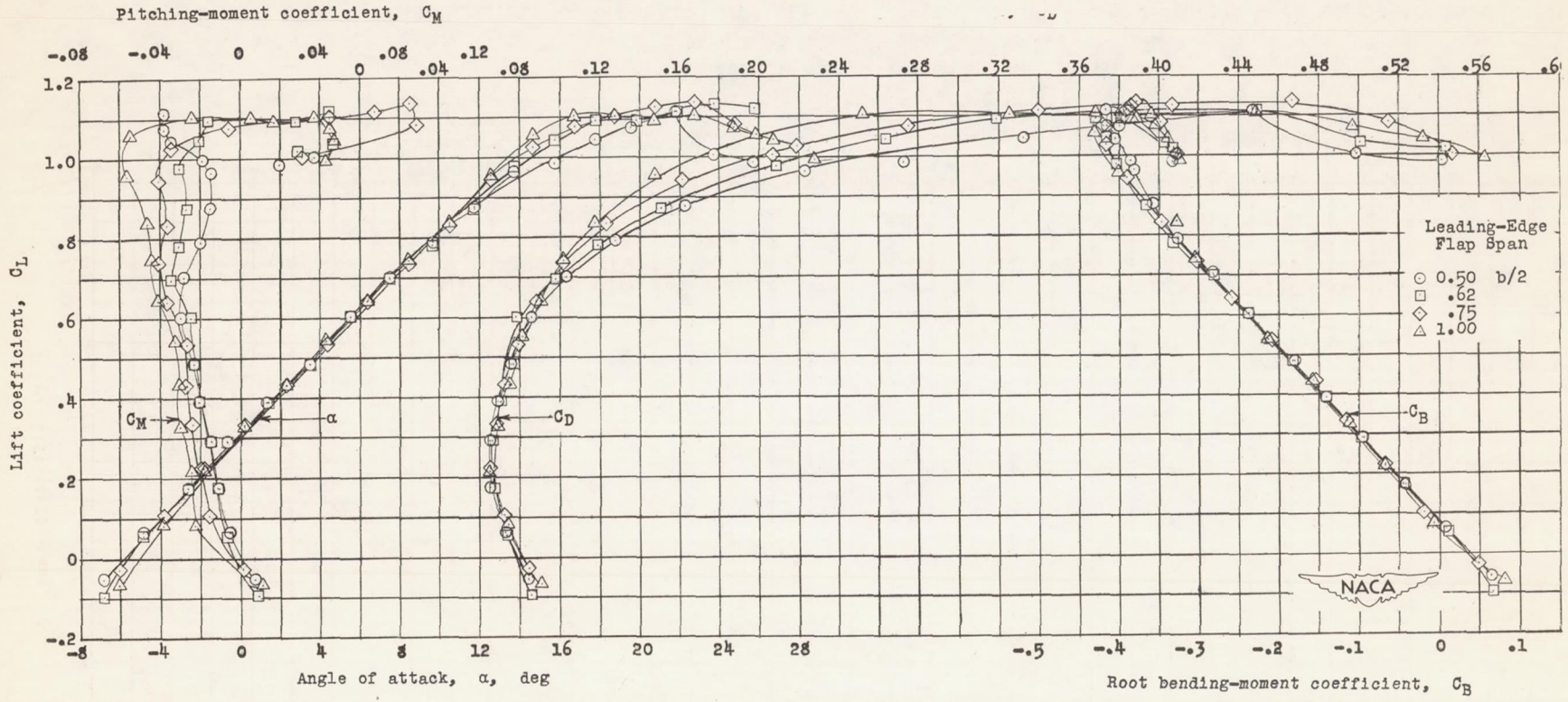

(b) Wing with $0.50\frac{b}{2}$ split flap, smooth.

Figure 14.- Concluded.

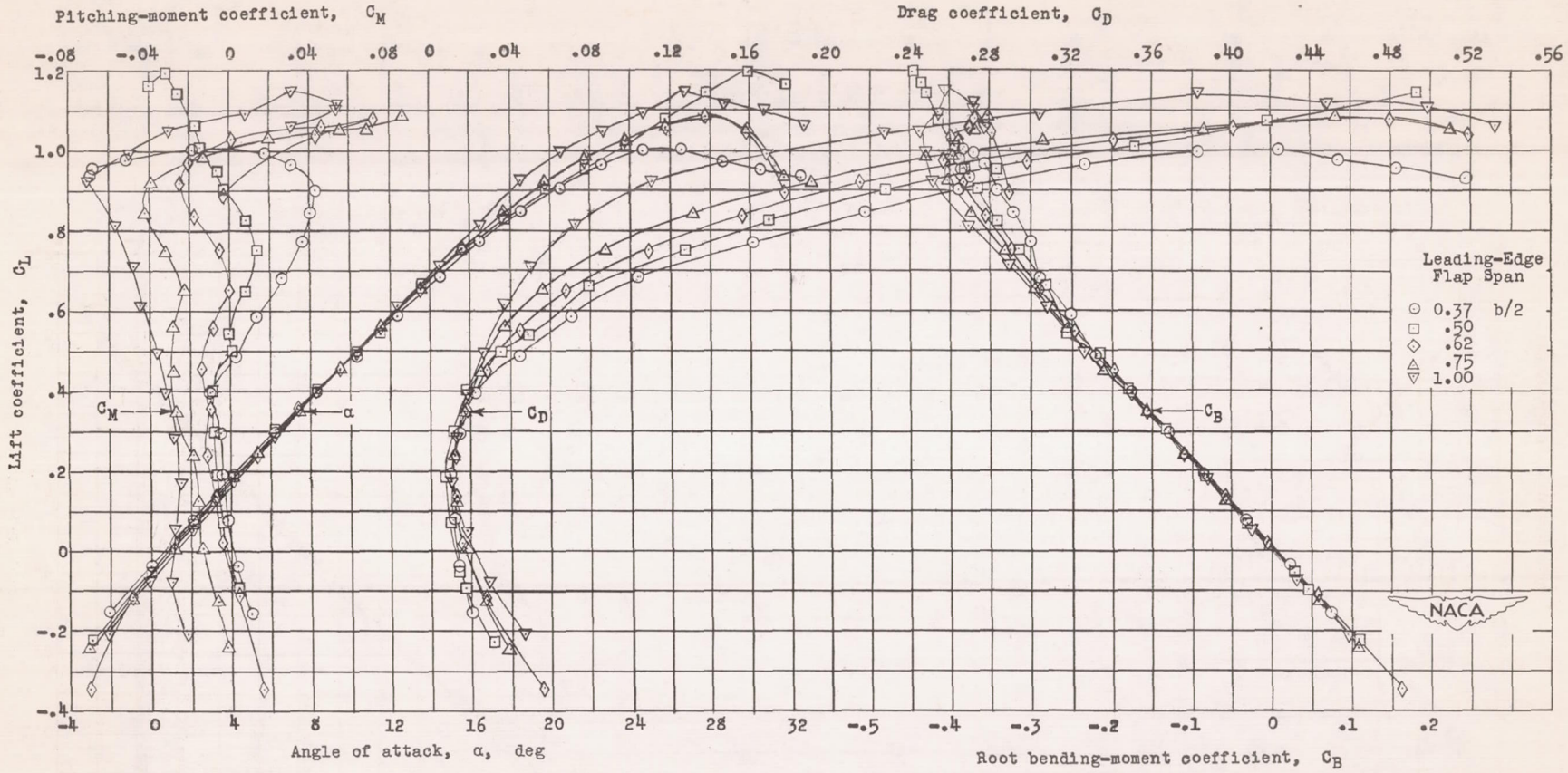

(a) Plain wing, smooth.

Figure 15.- Low-speed aerodynamic data for the 45-4-0.6 wing with leading-edge flaps of various spans deflected 30°. R = 4.5 × 10⁶.

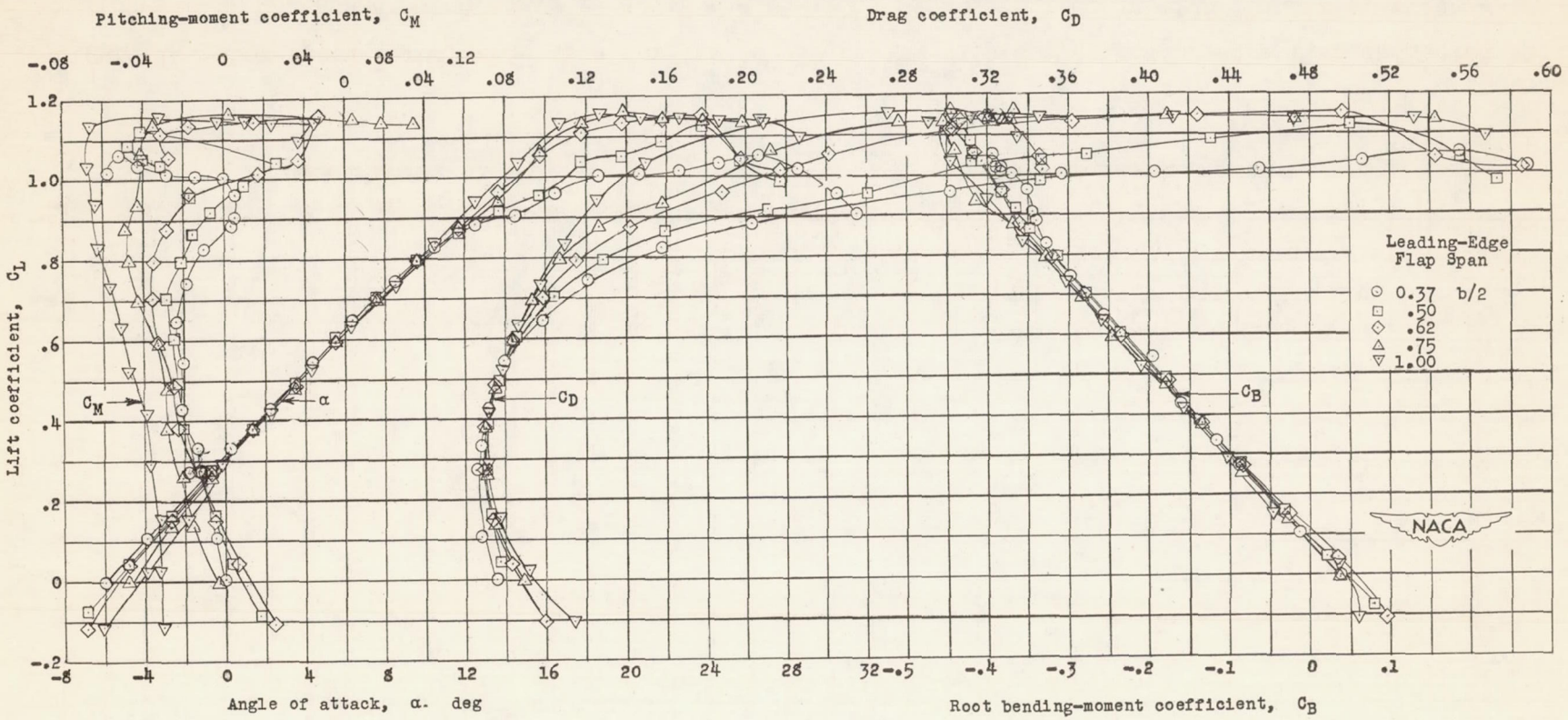

(b) Wing with $0.50\frac{b}{2}$ split flap, smooth.

Figure 15.- Concluded.

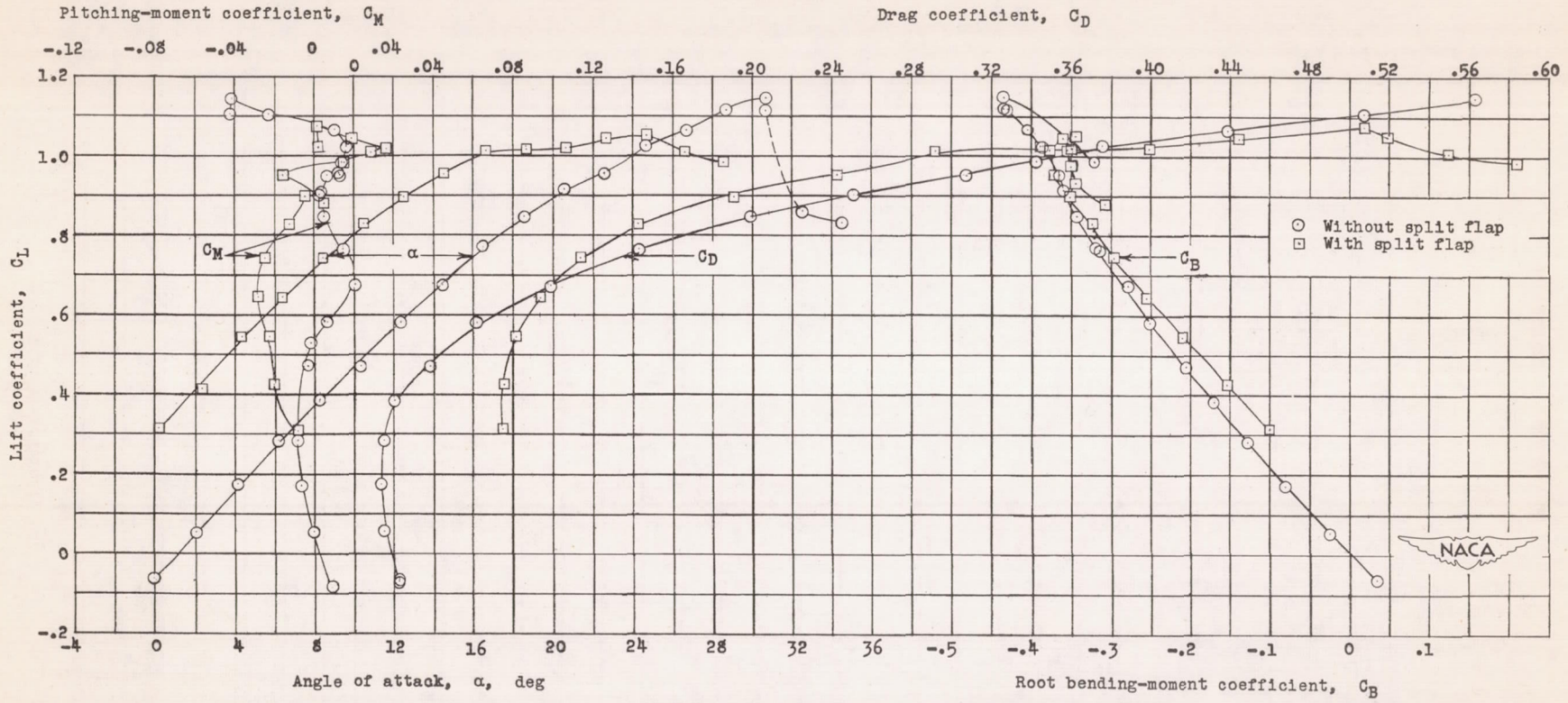

Figure 16.- Low-speed aerodynamic data for the 45-4-0.6 wing with $0.50\frac{b}{2}$ leading-edge flap deflected 40°. $R = 4.5 \times 10^6$.

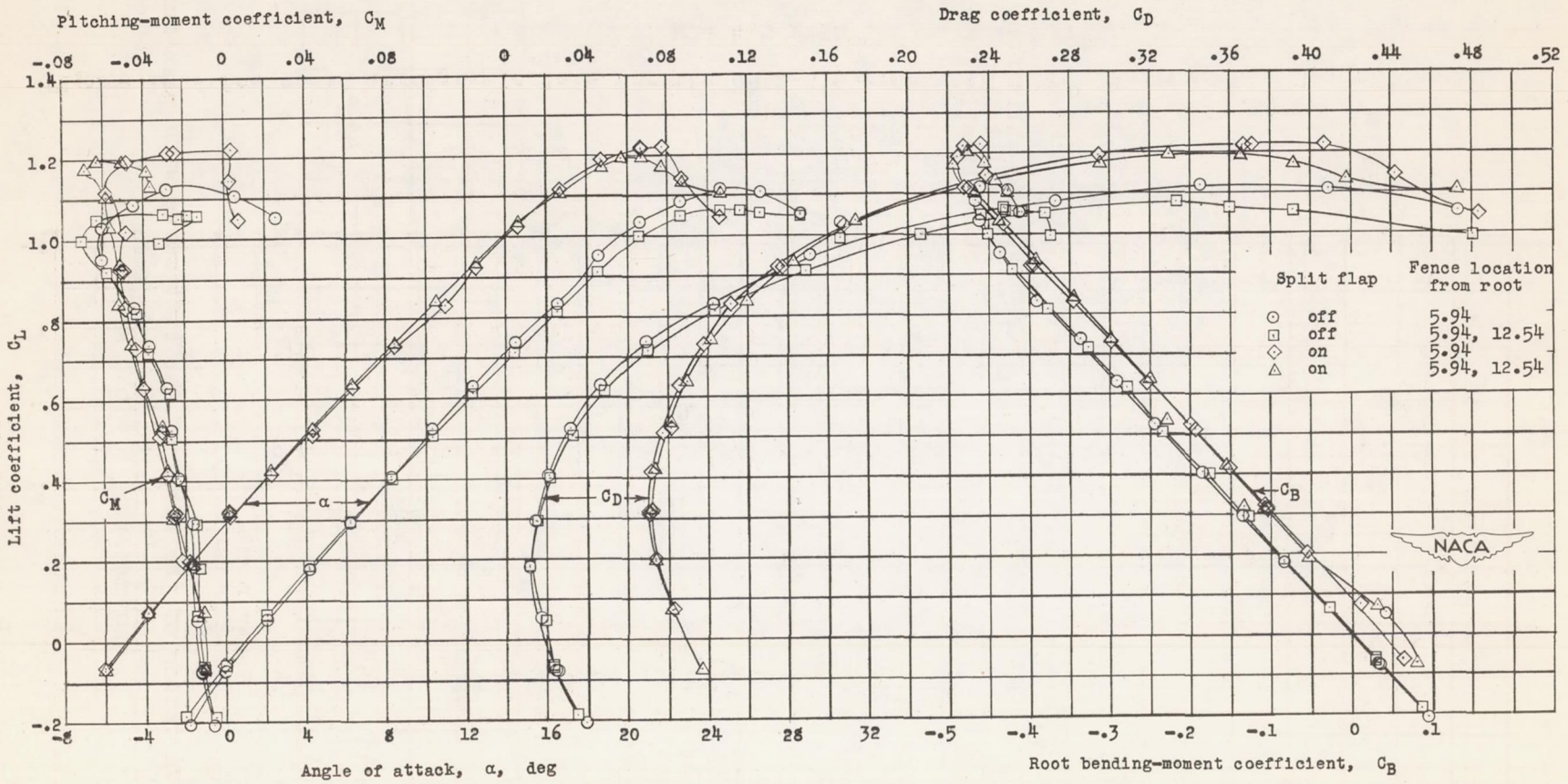

Figure 17.- Low-speed aerodynamic data for the 45-4-0.6 wing with $0.75\frac{b}{2}$ leading-edge flap deflected 30° with fence. $R = 4.5 \times 10^6$.

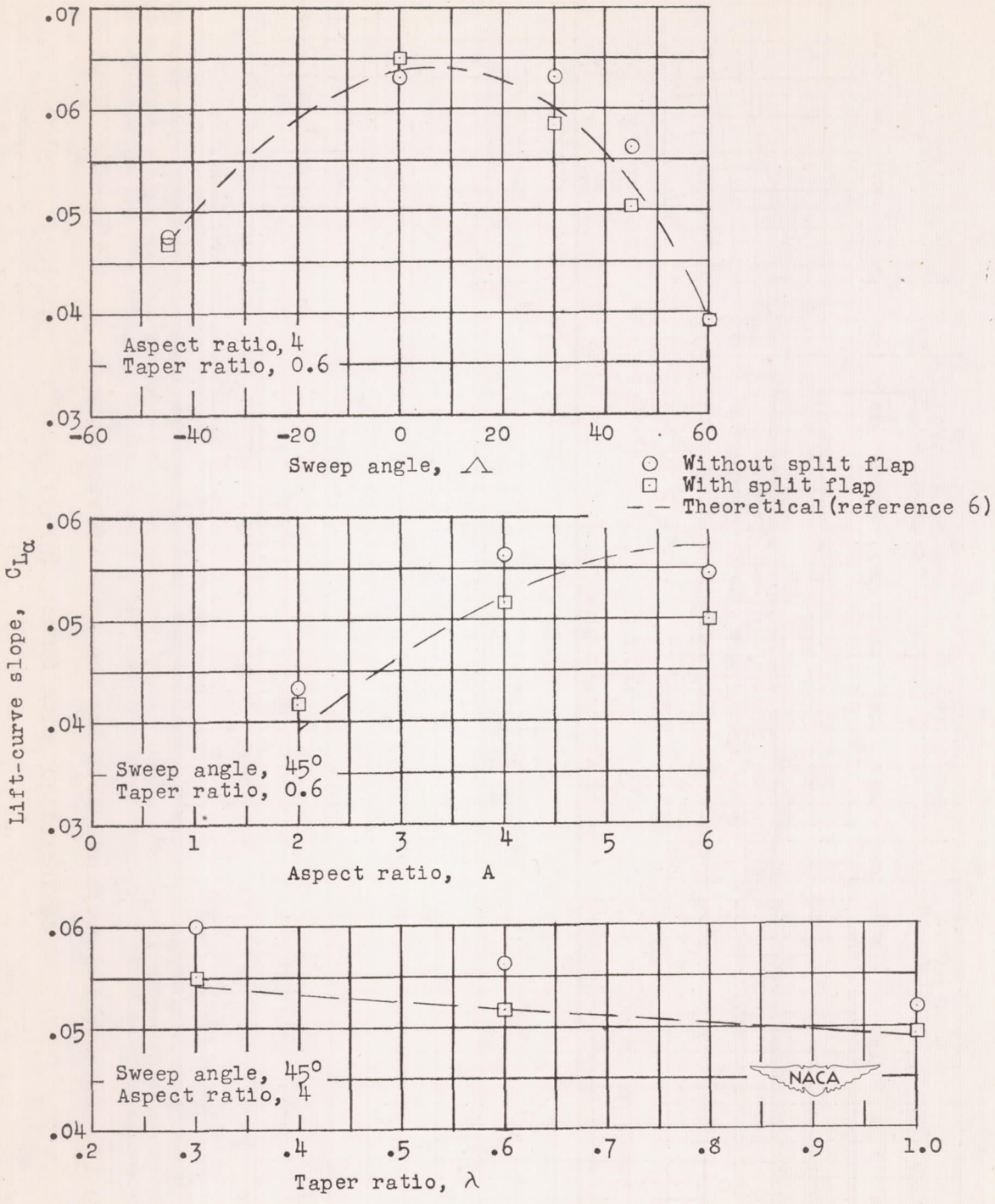

Figure 18.- Variation of the slope of the lift curve with plan-form parameters. $R = 6.0 \times 10^6$.

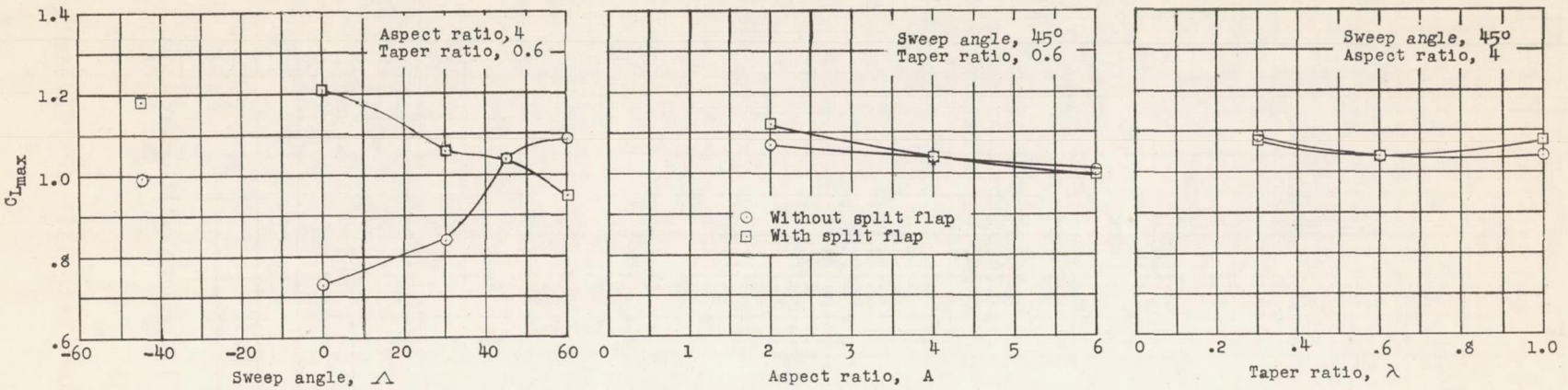

(a) Maximum lift coefficient.

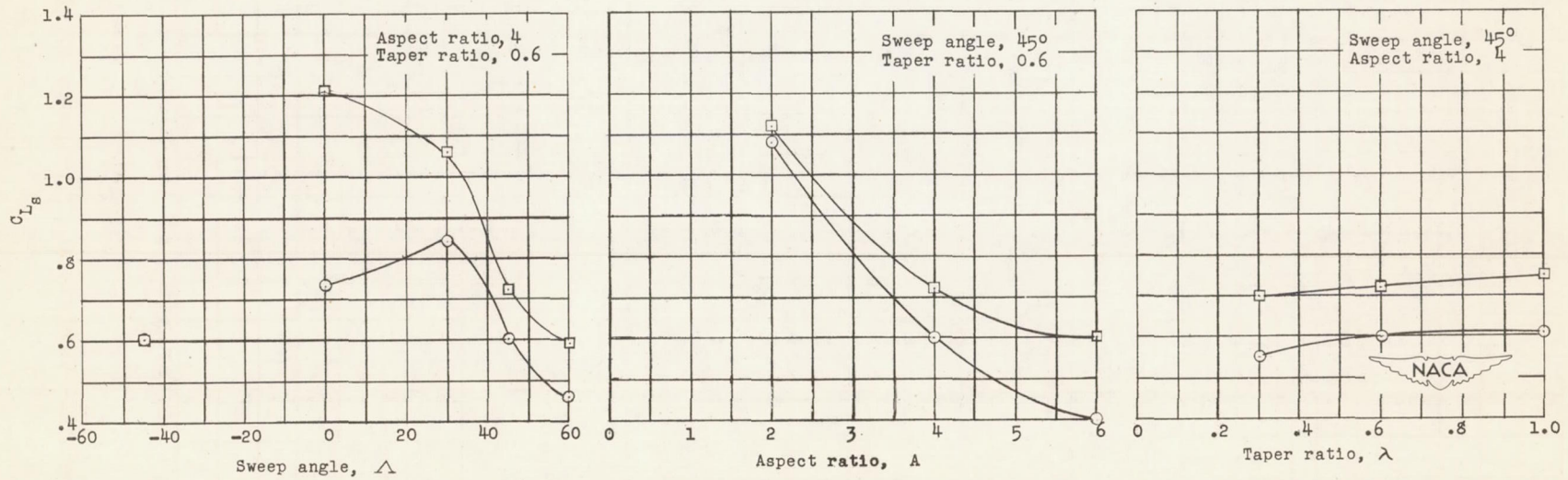

(b) Highest lift coefficient reached before unstable pitching-moment break.

Figure 19.- Variation of lift coefficient with plan-form parameters. $R = 3.0 \times 10^6$.

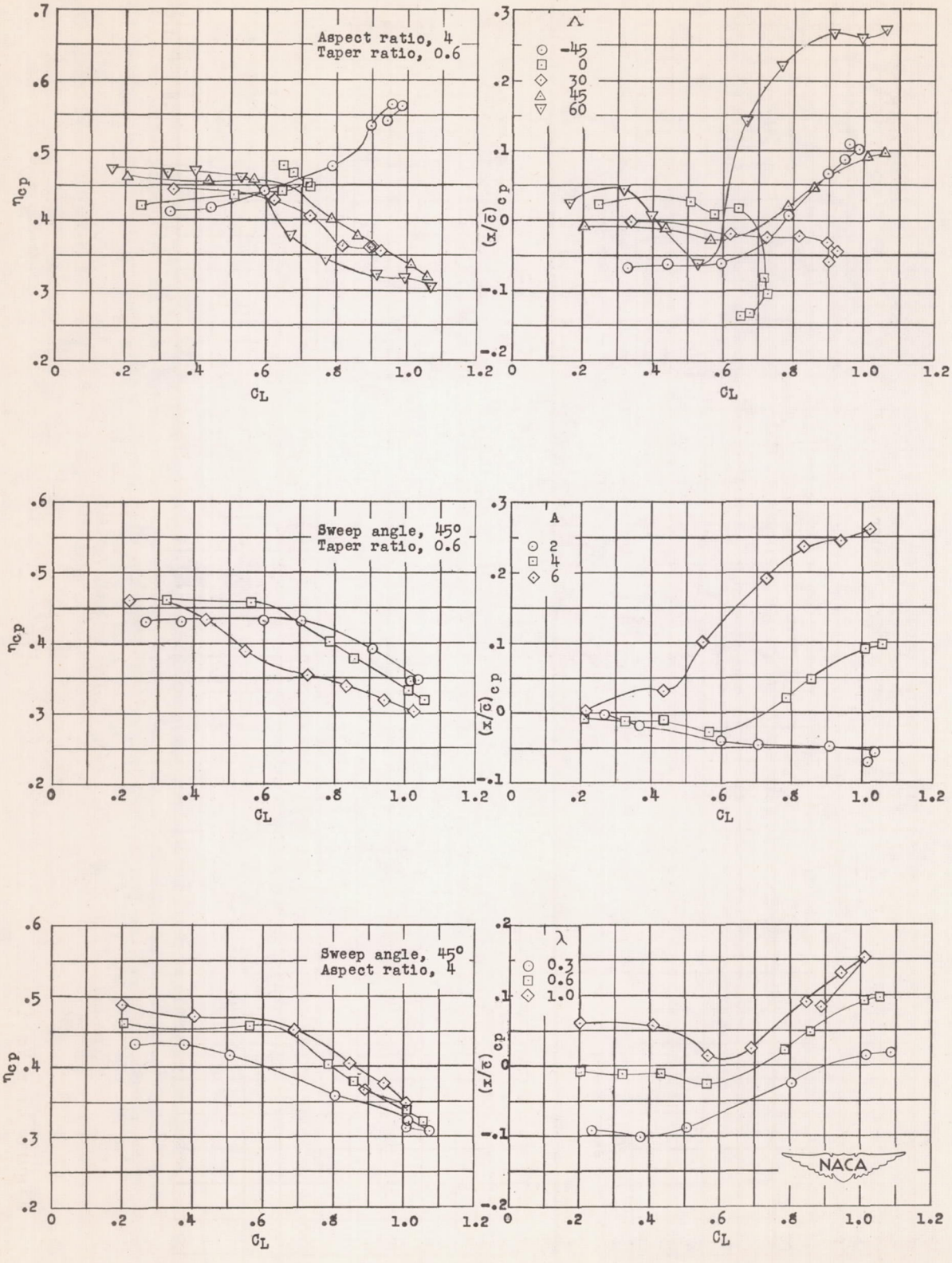

Figure 20.- Variation of centers of pressure with lift coefficient. $R = 6.0 \times 10^6$.

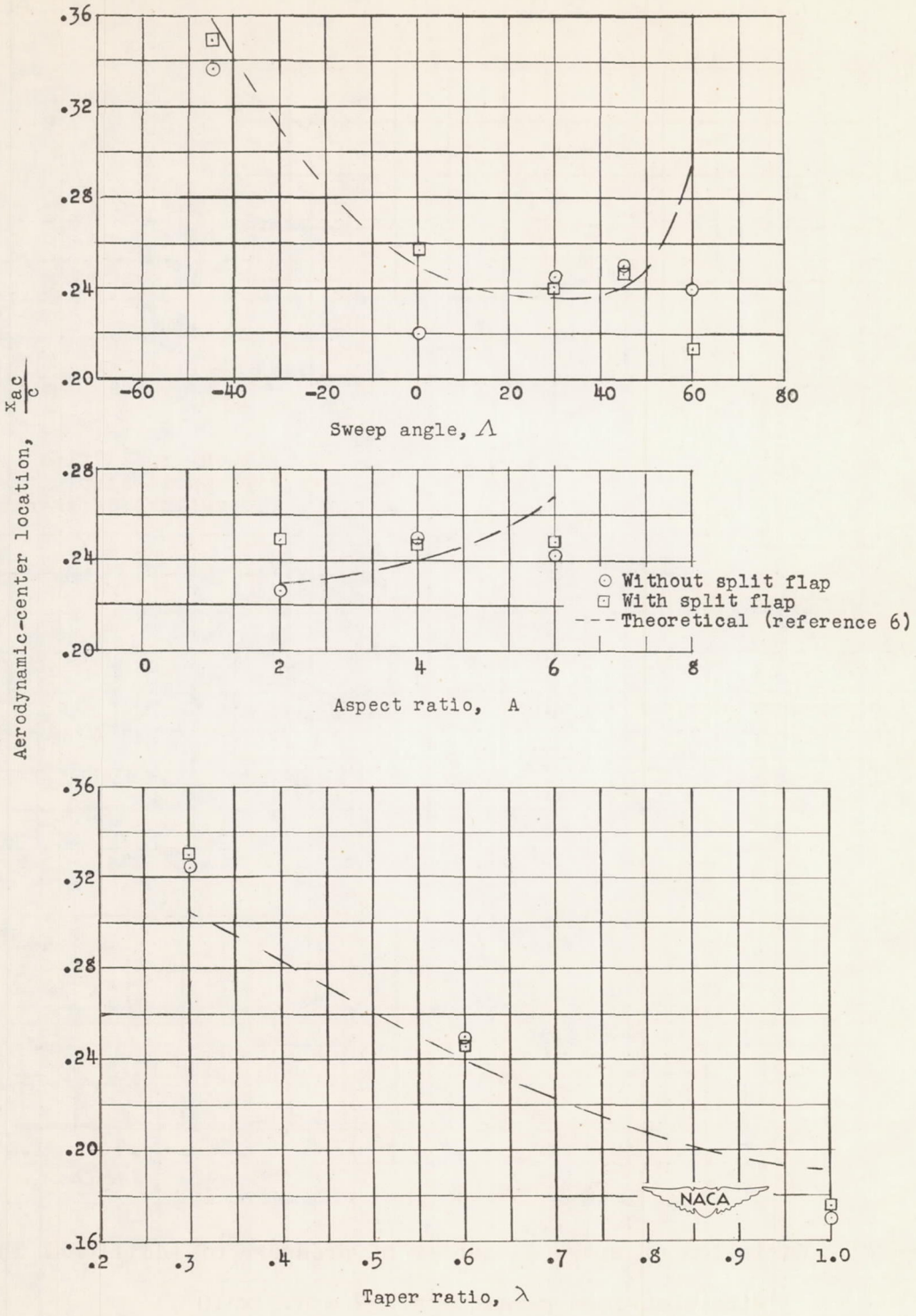

Figure 21.- Variation of aerodynamic-center location with plan-form parameters.

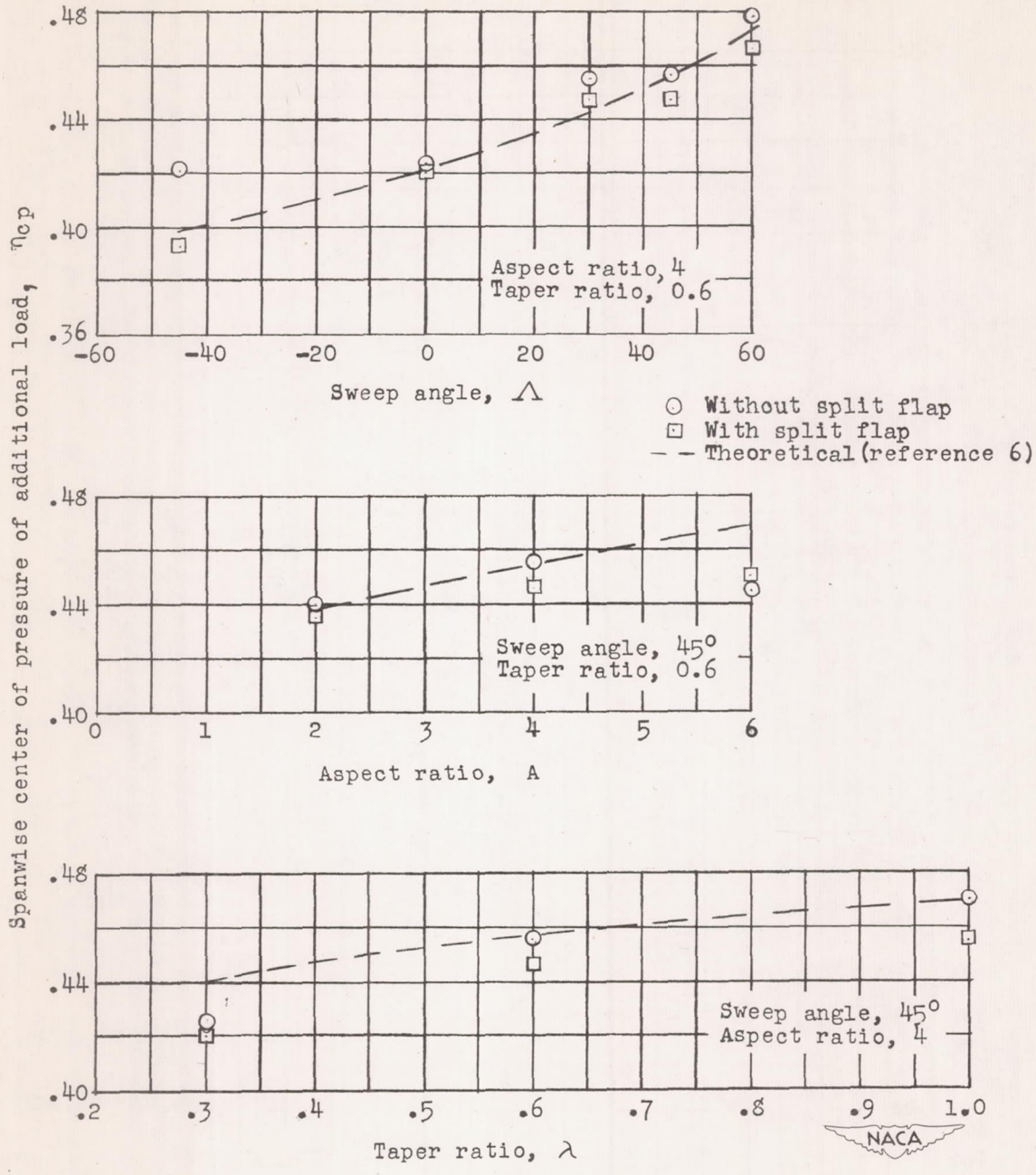

Figure 22.- Variation of spanwise center of pressure of additional load with plan-form parameters. $R = 6.0 \times 10^6$.